2011

NANOSTRUCTURED ANTI-BIOFOULING SURFACES: PHYSICAL DEPOSITION OF PS-*b*-PAA LANGMUIR-BLODGETT FILMS

David Bello
University of Rhode Island, david.g.bello@hotmail.com

NANOSTRUCTURED ANTI-BIOFOULING

SURFACES: PHYSICAL DEPOSITION OF PS-*b*-PAA

LANGMUIR-BLODGETT FILMS

BY

DAVID G. BELLO

A DISSERTATION SUBMITTED IN PARTIAL FULFILLMENT OF THE

REQUIREMENTS FOR THE DEGREE OF

MASTER OF SCIENCE

IN

CHEMICAL ENGINEERING

UNIVERSITY OF RHODE ISLAND

2011

MASTER OF SCIENCE THESIS

OF

DAVID BELLO

APPROVED:

Thesis Committee:

Major Professor_____Geoffrey D. Bothun_____

_____Richard Brown_____

_____Keunhan (Kay) Park _____

_____Nasser H. Zawia_____
DEAN OF THE GRADUATE SCHOOL

UNIVERSITY OF RHODE ISLAND
2011

ABSTRACT

Biofouling, the accumulation and proliferation of microorganisms, plants, and fouling animals on surfaces in an aqueous environment, poses a significant challenge. For example, the effects of fouling of ship hauls include hydrodynamic drag, increase in fuel consumption by ships whose hulls have been fouled, and increase in frequency of dry-dock cleaning.

In the history of marine navigation, varieties of anti-biofouling control measures have been suggested but tributyltin self-polishing copolymer (TBT-SPC) paints have been the most effective and commercially viable option in curbing biofouling. However, leaching of tri-organotin biocides from TBT-SPC paints through self-polishing activity constitute pollution which led to the ban of biocide-base paints. We explored bio-inspired nature of lubricin and fabricated polyelectrolyte polymer brushes from commercially available polymer materials by Langmuir-Blodgett deposition technique (LB fabrication) in order to control grafting density and by ATRP.

Interfacial tension results indicate that PS_{60}-b-PAA_{29}, based on steric and electrostatic interaction within the block copolymer, is very stable over ranges of pHand temperatures similar to that of the marine ecosystem. Fluorescence microscope and atomic force microscope imaging, as well as, advancing contact angle measurements on the physically fabricated samples shows that there was successful fabrication of PS_{60}-b-PAA_{29}brushes on glass surfacevia Langmuir-Blodgett deposition.

While biofouling test is underway on the brushes fabricated by LB deposition technique, preliminary biofouling testing by M. Callow's laboratory at the University of Birmingham on ATRP samples indicates that grafting duration (hence, thickness) of polyelectrolyte polymer brush has a direct impact on the film efficiency against biofouling.

ACKNOWLEDGMENTS

I would like to thank my Major Professor, Dr. Geoffrey. D. Bothun, a very kind, nice, and knowledgeble person who was interested in my success and accomplishment as long as I was willing to try and work hard. His support on many fronts made it possible for me to complete my Master's degree with good success.

I am indebted to Qian Ni for her help at the beginning of my graduate research experiments and her technical support while I was taking over the ATRP chemical deposition of the polymer films. It is my pleasure to thank Ed Baker at URI Aquarium for his technical support with regards to biofouling studies. Andrew Gauffreau, a student Mechanical, Industrial, and System Engineering Department, was also very helpful with AFM instrumentation. Also, Paul Johnson of GSC was terrifically helpful with fluorescence microscopy operations and trainings.

Finally, I appreciate Dr Sze Yang (Department of Chemistry) who gracefully served as the chair of my thesis committee, Dr. Park (Mechanical, Industrial, and System Engineering Department-thesis committee member), and Dr. Richard Brown (Chemical Engineering Department-thesis committee member) who has been very graceful towards me since the day I stepped on URI Campus.

DEDICATIONS

I dedicate this Master's Thesis to the Lord Jesus Christ through whom I can do all things because He strengthens me.

I also dedicate this work to my lovely wife, Oladayo Adedoyin Bello, and my boys, Joshua and Joseph Bello, for their sacrifices and support during the grueling years of graduate school.

TABLE OF CONTENTS

PAGE

viii

LIST OF TABLES

LIST OF FIGURES

CHAPTER 1

INTRODUCTION

The deleterious environmental and economical effects of bio-fouling in water treatment plants, heat-transfer systems, and marine environments present significant challenges. Biofouling describes the deposition and proliferation of undesired microorganisms on surfaces that are in constant contact with water. Biofouling occurs when bacteria, algae, barnacles, fungi, and other fouling organisms adhere to a surface in an aqueous environment (Anderson et al, 2003). A main result of biofouling is hydrodynamic drag due to increase in surface roughness of ship hull which causes increase in fuel consumption. Table 1.1 shows the foul rating system used by the US Navy to classify degree of fouling.

Table 1.1: Foul rating (FR) index used by the US Navy (Schultz et al, 2010)

Description of condition	NSTM (Foul Rating (FR))
Hydraulically smooth surface	0
Typical as applied AF coating	0
Deteriorated coating or light slime	10-20
Heavy slime	30
Algae, weed and juvenile tube worm (soft) and/or infant calcareous growth	40-60
Calcareous fouling juvenile to medium	70-80
Heavy calcareous fouling - shell	90-100

Table 1.2: Fouling on Arleigh Burke-class destroyer (DDG-51) class hulls investigated by means of 320 individual inspections reports from January 1, 2004 to December 31, 2006.

	Class	(US)	Comment
The cost of propulsive fuel DDG-51 class hull	0	$11.1M	The baseline, hydraulically-smooth
Increasing fouling	FR -20-30	$330,000 - $440,000 per ship per year	Fuel consumption
Increasing fouling	FR-30	$1.15M per ship per year	Fuel consumption increase by 10.3%
Cost associated with hull fouling for the for the entire US Navy's DDG-51	Possibly 30 < FR < 60	$56M per year	Class with change in expenses due to paint, hull cleaning, or other management practices
Increasing fouling	FR-60	$119M	
Cost associated with hull fouling for the for the entire US Navy's ships	FR-60	$400M-$540M	Fleet wide annual cost due to fouling

In Table 1.2, different levels of fouling based on foul release classification with associated cost are presented. It costs the US Navy (US) $11.1 million to move Arleigh Burke-class destroyer (DDG-51) class of ships whose hulls are hydraulically smooth and free from fouling. If the hulls were fouled at FR-20-30 level, the fuel cost increases by (US) $330,000 -$440,000 per ship per year. If the fuel consumption increases by 10.3% and with the level of hull fouling at FR-30, the cost of fuel consumption increases to (US) $1.15 million per ship per year. With increase in fouling to FR-60, the cost of fuel usage and expenses due to hull cleaning, hull paint,

and other maintenances of the ship could be as much as (US) $56 million per year or up to (US) $119 million. Finally, the fleet wide annual cost due to fouling at FR-60 was estimated to be (US) $400 million -$540 million (Schultz et al, 2010).

In order to combat bio-fouling, biocides are used in surface coatings. However, biocides themselves are toxic and constitute pollution when leached from the surface. Hence, there is a need to develop non-toxic antifouling surfaces that are economical and scalable. Nanostructured polymer brush coatings may provide such a surface by engaging steric and electrostatic repulsive forces in order to prevent biofouling.

Research objectives

This work is driven by the hypothesis that polyelectrolyte brushes can be fabricated from inexpensive commodity polymers and exhibit antifouling properties through engineered steric and electrostatic interactions combined with nanoscale topography. It has been derived from ongoing collaboration and support through the Naval Undersea Warfare Center (NUWC). To test this hypothesis, we have examined the fabrication of self-assembled amphiphilic block co-polymer brushes composed of poly(styrene)-block-poly(acrylic acid) (PS-*b*-PAA). The brushes were formed via physical Langmuir-Blodgett deposition on prepared glass slides as model surfaces. This method (among others such as thermal evaporation, electrodeposition, and sputtering) was chosen because it enables us to control the monolayer thickness, as well as, surface coverage.

The main objectives of this M.S. project are stated below:

1. Examine the surface activity of PS-*b*-PAA at air/water interfaces under relevant system conditions. The premise behind this objective was to examine *a priori* the surface pressure of the brushes before depositing them on the substrates. Previous work has shown that film structure at an air/water interface can be transferred onto solid substrates (Currie et al, 2000).

2. Examine the effect of substrate treatment and preparation on PS-*b*-PAA film deposition. The premise behind this objective was to identify the best surface treatment and preparation method to achieve physisorption of PS-*b*-PAA film onto the substrate.

3. Fabricate and characterize physically-deposited PS-*b*-PAA brush coatings on prepared substrates as a function of surface pressure, which sets film morphology. Characterization was conducted using atomic force microscopy AFM), surface pressure-area isotherm studies, and Uv-vis fluorescence spectroscopy.

4. Fabricate covalently grafted PAA and PS-*b*-PAA by atom transfer radical polymerization (ATRP), consistent with previous work by Qian Ni, and test the bio-fouling properties of these coatings in Professor Callow's laboratory at The University of Birmingham, UK. This work was intended to 1) test the performance of previously developed coatings and 2) provide a comparison between covalently and physically deposited brushes.

Chapter 2 presents the background of this project. It highlights the evolution of antifouling paints and focuses on the classifications of antifouling coatings such as non-biocide based, biocide-based, and non-toxic technologies.

Chapter 3 itemizes the materials used in this research and explains the methods used. It highlights the surface pre-treatment steps, hydroxylation, application of primer to the surface of the substrate, preparation of the copolymer solution, and explains how to physically deposit PS-*b*-PAA.

In Chapter 4, results and discussion are presented in detail. This includes an interpretation of the results from surface pressure-area isotherms, contact angle measurements, UV-vis measurements, and fluorescence microscope images. Conclusions drawn will be presented in chapter 5.

Finally, historical development in monolayer science, information about monolayer characterization, calculation of the volume of the block copolymer required, and detailed description of instrumentations are provided as Appendices.
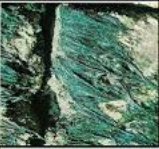
CHAPTER 2

REVIEW OF LITERATURE

Targeted biofouling organisms

Marine or freshwater structures such as oilrig platform supports, ship hulls, cooling systems for power plants, culture rafts, and ocean thermal energy conversion systems are usually protected against fouling by coatings with compounds that deter settlement of fouling species (Stupak et all, 2003).

Table 2.1: Survey and characteristics of major biofouling organism species from plants to invertebrate animals (Almeida et al, 2007).

Groups	Algae (plants)	Invertebrates (animals)							
Subgroups	(a) green, (b) brown and (c) red	Hard shell organisms				Grass type organisms	Small bush organisms	Spineless organisms	
Designation	(a) Enteromorpha, Ulva and Cladophora), (b) (Ectocarpus and Fucus, and (c) (Ceraminum)	Balanus	Barnacles	Molluscs	Fouling bryozoans	Hydroids or bryozoans	Hydroids or bryozoans	Ascidians	Sponges and sea anemones
Example of typical aspect									
Designation	Green algae	Balanus	Calcareous polychaetes	Molluscs	Fouling bryozoans		Bryozoans	Ascidians	
Example of typical aspect									
Short description	Only plants that become attached to immersed surface: a) close to surface; b) at mid depth; and c) at depth	Attached trunco-conical or cylindrical crustaceans	Barnacles are Balanus that are fixed to surfaces via a stem	Bivalves containing a spineless animal in their interior	Calcareous incrustations that multiply from a central individual	Organisms that cover surfaces with an open grass or fur	Like bushes of several centimetres and with branches	Constituted by a spineless bag with two tubular openings or starry plates	Spineless and spongy aspect (sponges) and sea anemones

The microorganisms that cause fouling are small in size when viewed individually, frail in nature, and well adapted to aqueous environments. However, the effects of their activities are very profound economically and environmentally. Examples of fouling organisms are presented in Table 2.1. The scale of sizes of fouling organisms has been developed by (Magin et al, 2010) as shown below.
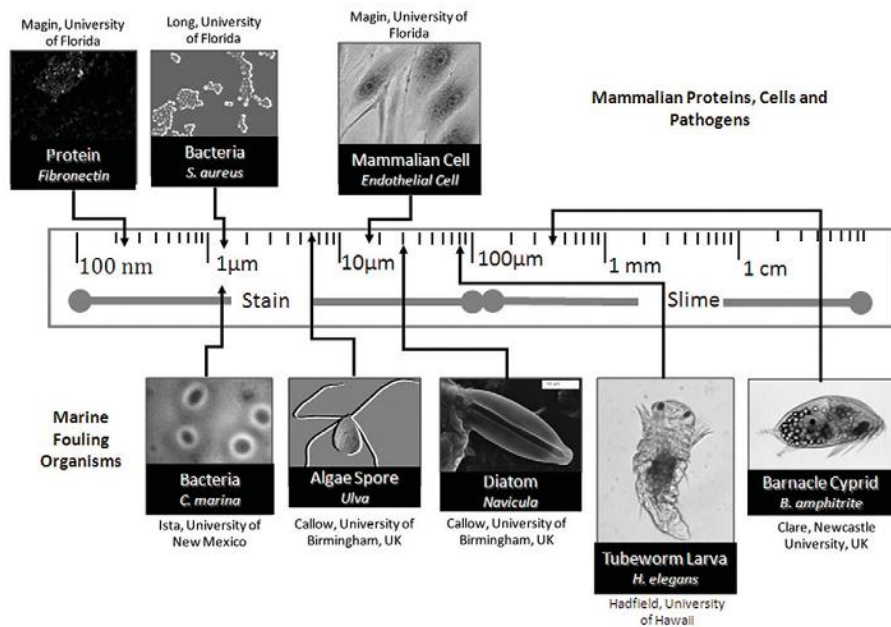
Figure 2.1: Hierarchy of fouling organisms in marine and biomedical environment

It has been estimated that the weight of fouling organisms could be about 150 kg/m^2 when they completely cover a surface. This is equivalent to approximately 6000 tons of fouling materials. Typically, for large commercial vessels, the hull has an approximate surface area of about 40,000 m^2 (Howell et al, 2009). Consequently, the effective weight of the ship will be increased causing hull roughness, loss of velocity, reductions in fuel efficiency, and pollution due to greenhouse gas emission.

7

Antifouling coatings classifications

Classification of antifouling mitigation coatings

In order to control fouling, various methods have been used over the past centuries. Antifouling coatings can be classified into three major categories: biocide-based antifouling coating, biocide-free antifouling coating, and non-toxic technology. The most successful method is the incorporation of additives with biocidal effects into antifouling paints.
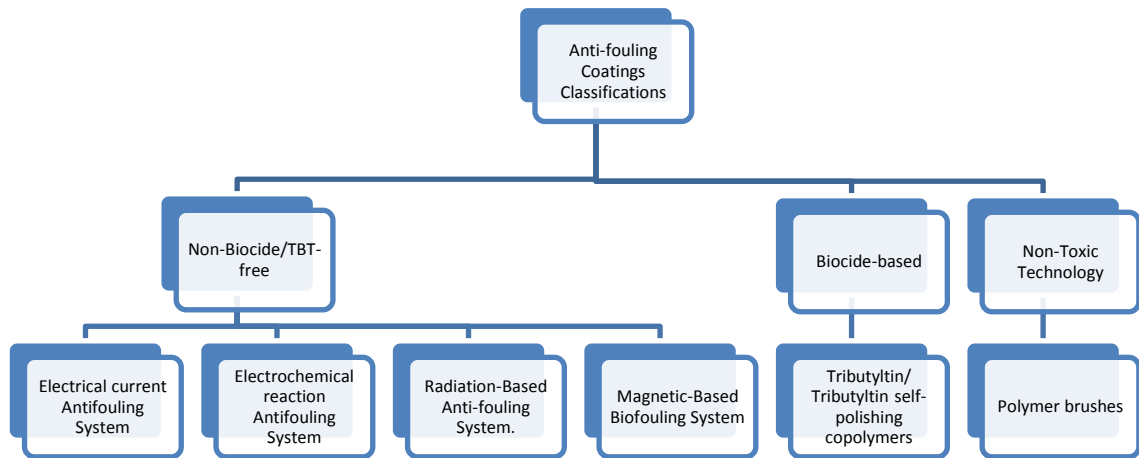
Figure 2.2: Classification of antifouling mitigation coatings.

Non-biocide/tributyltin-free antifouling systems

Due to marine pollution caused by leaching of organotin (in the form of tributyltin) compounds, copper, zinc, lead, nickel, arsenic, alloys of antimony, and galvanized iron found in biocide-based antifouling paints, attempts have been made to develop tributyltin-free antifouling coatings. Examples of tributyltin-free antifouling

systems are electrical current antifouling system, electrochemical reaction antifouling system, and radioactive antifouling system.

Electrical current antifouling system (ECAS)

Electrical antifouling alternative involves the use of electricity to produce toxic chemicals such as chlorine on ship hulls (Iselin, 1952; Swain, 1998; Huang, 1999). This results in large voltage drop and corrosion of the surface of the ship hull. In addition, this method causes release of chlorine and organic chlorine derivatives into the ocean leading to localized pollution. Another disadvantage of this method is that uniform dispersion is not feasible leading to inefficient antifouling control (Bertram, 2000).

Electrochemical reaction antifouling system (ECRAS)

ECAS is environmentally unsafe and inefficient. This was one of the main reasons for exploring alternative means of controlling biofouling using the principle of electrochemical reaction to attack fouling organisms. This system uses electron transfer between an electrode and microbial cells resulting in electrochemical oxidation of the intracellular substances (Yebra et al, 2004). Other electrochemical systems used involve the development of conductive paint electrodes that were used to create an electrical potential (Okochi et al, 1995). The effect of the electrical potential is that it killed bacteria and fluctuation of the electrical potential to negative value causes the bacteria to be removed from the electrodes because most bacterial are negatively charged. ECRAS has some limitations. For instance, it is restricted to

small scale applications such as control of bacteria fouling (among all fouling organisms) in pipes.

Radiation-based antifouling system (RBAS)

Due to the limitation of ECRAS mentioned above, investigators experimented with radiation-based antifouling system. An example of RBAS includes acoustic radiation (applied by vibration of piezoelectric coatings). Ultra-violet radiation has also been used for sea water sterilization (Swain, 1998). However, the power requirement of this technology is enormous (Swain, 1998); therefore it is not commercially feasible for large scale application.

Biocide based antifouling systems

Early biocide-based antifouling paints contain biocides such as copper, arsenic or mercury oxide. For example, copper is commonly used in antifouling paints as a metal, oxides, sulfides, and thiocyanates (Ranke et al, 1999). Another component of antifouling paint is zinc pyrithione. It is used as the active ingredient in anti-dandruff shampoo and certain antifouling pigments (Ranke et al, 1999). Other biocide-based antifouling paints contain naphtha or benzene (Iselin, 1952). In 1958, it was discovered that tributyltin acrylate ester can be used as an antifouling coating (Gitlitz et all, 1981). For instance, tributyltin acrylate and tributyltin methacrylate were known to be very potent against marine biofouling (Yebra et al, 2004). However, control of marine fouling through antifouling paint application was revolutionized by discovery of tributyltin-self polishing copolymer (TBT-SPC). TBT-SPC antifouling

paints contain polymer backbones linked to tributyltin by an ester linkage (Figure 2.3) (Anderson, 1995). The hydrophobic nature of tributyltin prevents water from penetrating through the coating.

In sum, all biocide-based antifouling paints contain at least one or more of the following active ingredients: zinc pyrithione, naphtha, benzene, tributyltin acrylate ester, tributyltin acrylate, tributyltin methacrylate, tributyltin self-polishing copolymers, and combination of copper with metals, oxides, sulfides, and thiocyanates. These ingredients confer toxicity on the antifouling paints that contain them. Therefore, due to the leaching of these toxic ingredients into the marine environment, regulations were enacted to ban their use. The ban has motivated researchers to look for environmentally benign alternatives to biocide-based antifouling coatings.
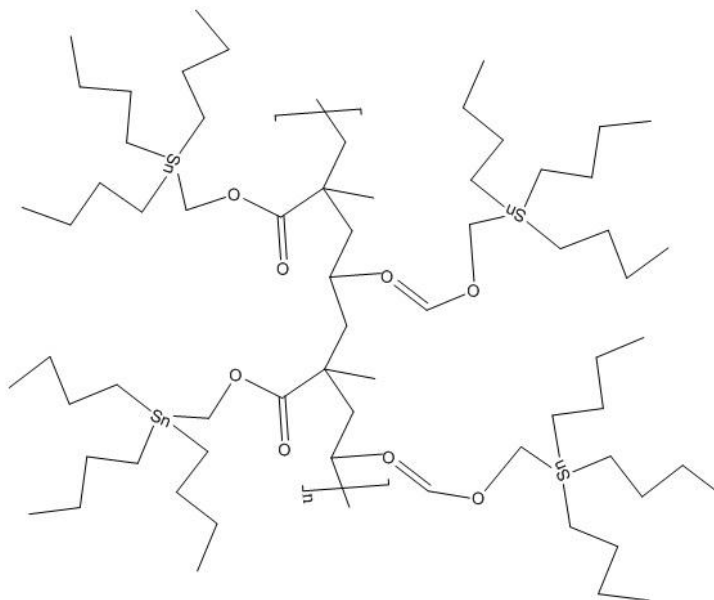
Figure 2.3: Structure of tributyltin copolymer used as self-polishing copolymer in biocide-based antifouling paints.

Non-toxic technology antifouling system

The antifouling alternatives described thus far either have environmentally negative impacts or economic limitations that cause regulators or the ship industry to restrict their use. A good antifouling alternative must not be toxic, should not be expensive, should not be chemically unstable, and finally, it must be able to prevent fouling from any organism regardless of the species (Chambers et al, 2006).

Some non-biocidal alternatives meet the requirement stated above. Non-toxic coatings can be divided into three broad categories, namely (a) foul release coatings, (b) smart coatings, and (c) hard marine coatings (Howell et al, 2009).

Foul-release coatings

Foul-release coatings are coatings that render a surface non-stick and extremely smooth; they confer low friction and low-surface energy characteristics on a surface, thus arresting the formation of biofilm on surface structures that are in contact with water by marine fouling species (CEPE Antifouling Working Group, 1999; Chapman, 2003; Howell et al, 2009).

Smart coatings

Smart coatings are materials that provide specific response to certain external stimuli. In other words, smart coatings can sense their environment and respond appropriately to the stimulus (Baghdachi, 2009). Such stimuli or environmental conditions could be temperature, stress/strain, pH, and ionic strength. Examples of smart coatings are antifouling applications, antimicrobial (in the medical field),

stimuli response coatings, self-healing surfaces, self-cleaning, and super hydrophobic/hydrophilic switching coatings (Baghdachi, 2009; Yebra et al, 2004).

A much broader categorization of smart coatings are bioactive coatings (antimicrobial polymers, antifouling coatings, and photocatalytic coatings), nanotechnology-based coatings (self-assembling polymers and coatings, photonics, and molecular electronics), stimulus and response coatings (coatings functioning as sensors, color shifting coatings, and light sensing coatings) and self-assembled intelligent layers (self-repair and healing coatings, super hydrophobic coatings, and molecular brushes) (Tanner, 2005).

Polymer Brushes

Polymer brush describes an arrangement of bulky, polymer macromolecules (consisting of repeated units) that are physically or chemically anchored to a surface on one end. Not all polymer chains immobilized to a surface are polymer brushes. In a polymer brush arrangement, the grafting density is high enough such that the polymer chains are forced to stretch (Zhao et al, 2000).

Polymer brush arrangement confers special characteristics that can be explored in a number of applications such as adhesive materials (De Gennes et al, 1992; De Gennes et al, 1993), surface coatings that controls depositions of biocolloids like protein adhesion to a surface (Amiji et al, 1993; Currie et al, 2002), and as lubricants (Joanny, 1992). They can also be used as chemical gatekeepers and nanomaterial triggers that initiate drug delivery under certain conditions.
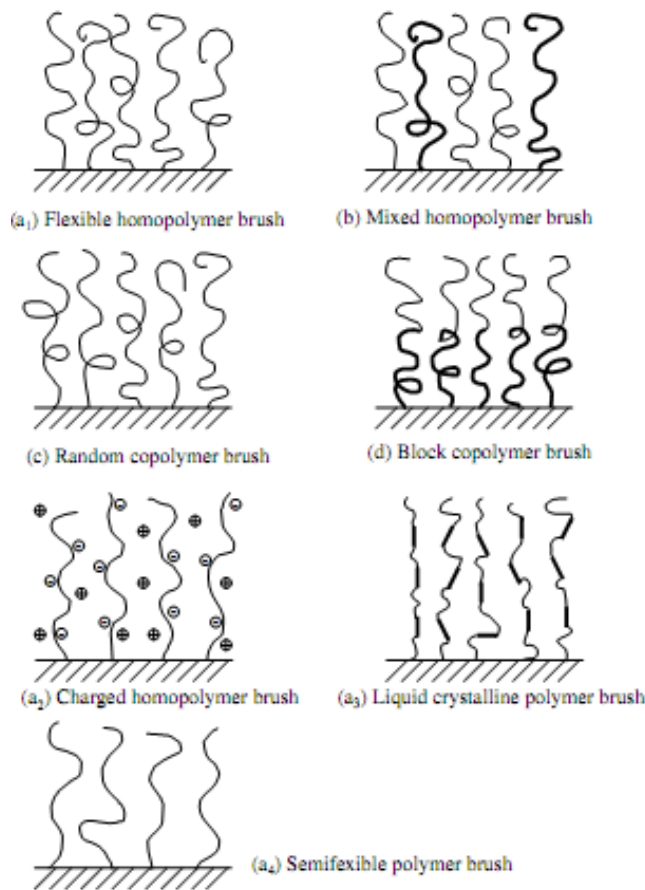
Figure 2.4: Polymer brush classification based on their compositions (Zhao et al, 2000).

Figure 2.4 presents the classification of polymer brushes based on their compositions (Zhao et al, 2000); homopolymer, mixed homopolymer, random copolymer, and block copolymer brushes. Homopolymer brushes are immobilized polymer chains that consist of one type of repeating monomers, mixed homopolymers brushes, on the other hand, are made up of two or more homopolymer types. In random copolymer brushes, the chains have two different repeating units that are haphazardly distributed on the substrate's surface. Finally, block copolymer consist of two or more homopolymers that are covalently bonded to each other on one end while the other end is tethered to the supporting surface. Examples of surfaces that have

14

been modified with polymer brushes include gold, silver, glass/silicon wafers, and titanium (Raynor et al, 2009).

Polymer brush can also be categorized into different classes based on the type of interaction between the brush and its environment as shown in Figure 2.5 (Toomey et al, 2008). The category would be classical if the interaction of the brush with the environment can based on van der Waals interaction or a system dependent criterion. On the other hand, we have a non-classical system if we cannot describe the interaction of the brush with its environment with a generalized model (Toomey et al, 2008).
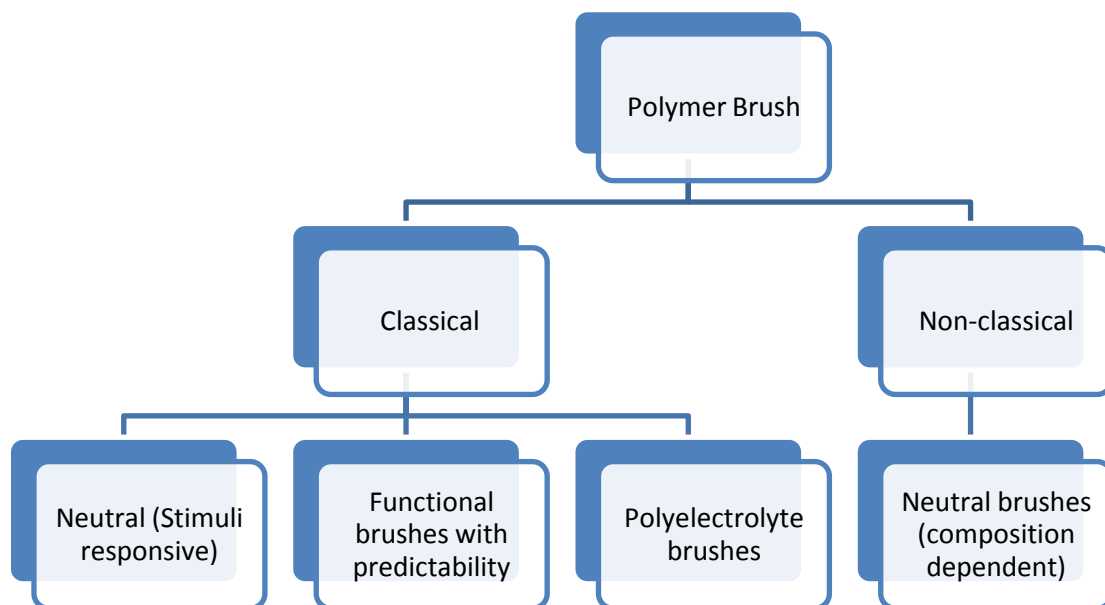
Figure 2.5: Alternative polymer brush classification based on the type of interaction between the brush and its environment.

Polymer brushes can either be prepared by physisorption or by chemical grafting. There are two types of chemical grafting methods, namely, "grafting to" and "grafting from". In the chemical grafting method, the polymers are attached to the surface and to each other via covalent bonding.

The "grafting to" approach of brush synthesis can be referred to as the top-down method in which the polymerization is performed first to form the polymer chains and then attached to the surface afterwards as shown in Figure 2.6. Specifically, monomers with reactive terminals are used in making the polymer chains. In order for the reaction to be successful, the surface on which the brush is to be grafted must be "activated" in order to accept the incoming polymer chains. One difficulty that is associated with this method of polymer brush fabrication is that after addition of few polymer chains, steric interaction may hinder available sites on the substrate surface from accepting other incoming chains.
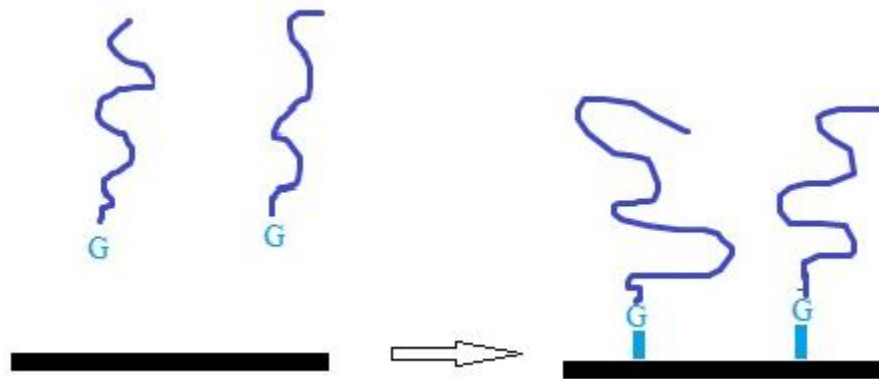
Figure 2.6: Schematic of the "grafting to" method of fabricating polymer brush. After addition of few polymer chains, steric interaction may hinder other incoming chains from being anchored to the surface.

The "grafting from" approach involves covalently binding monomers to the substrate surface and growing polymer chains from the anchored monomers through polymerization. It is possible to obtain high degree of polymerization and grafting density (Vos et al, 2009). The main challenge of both grafting methods is controlling the grafting density. Figure 2.7 shows the schematic of the "grafting from" method of fabricating polymer brush.
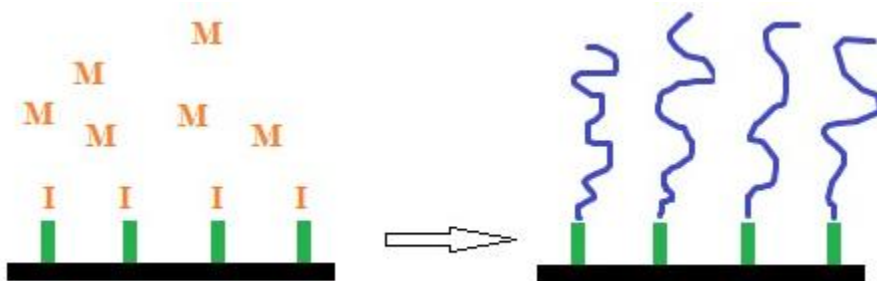
Figure 2.7: Schematic of the "grafting from" method of fabricating polymer brush.

Advantages and disadvantages associated with different methods of polymer brush fabrications have been summarized and they are presented in Table 2.2.

Table 2.2: Comparison of the advantages and disadvantages of using physical and chemical deposition techniques to prepare polymer brushes (Raynor et al, 2009).

	Physisorption	Chemisorption
Advantages	Simple formation especially alkanethiols on gold and chlorosilanes on oxides Molecularly well-defined layers End groups used to tailor surface properties, subject to modification with biological ligands	Long-term stability Options for preparation: grafting from grafting to Tunability through choice of monomer e.g., acrylates and styrenes Variety of polymerization methods SI-ATRP, ROP, NMP, cationic, and anionic Greater film thickness; control over brush length Thick film might provide self-healing of defects
Disadvantages	It is difficult to form bond between the polymer and the substrate Presence of pinholes and defects	More complex preparation More complex structure

Physisorption enables one to control the grafting density and surface coverage. In order to make the monolayer, a Langmuir-Blodgett trough (shown in Figure 2.8) can be used. First, a monolayer is prepared by spreading the surfactant, from which the polymer brush is to be made, on the surface of the subphase in the Langmuir-Blodgett trough. The spreading solvent is then allowed to evaporate from the subphase surface.
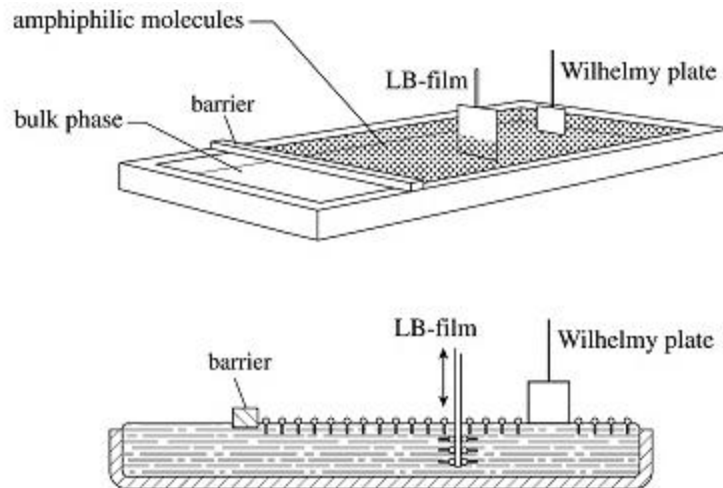
Figure 2.8: Schematic illustration of Langmuir-Blodgett deposition technique (Currie et al, 2002).
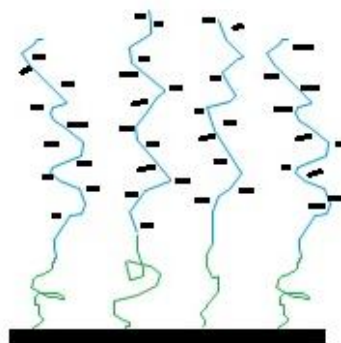
Figure 2.9: Diagrammatic illustration of polymer brush prepared by Langmuir-Blodgett deposition technique.

A substrate that has been pre-treated is then dipped vertically (Langmuir-Blodgett technique) or horizontally (Langmuir-Schaeffer technique) into the monolayer. Upon withdrawing the substrate, polymer brush at the air/water interface is deposited on the surface of the substrate (Figure 2.9).

The block copolymer used in this research is a polyelectrolyte polymer brush (poly(styrene)$_{60}$-*block*-poly(acrylic acid)$_{29}$ (PS$_{60}$-*b*-PAA$_{29}$)). The major forces acting

within the chosen polyelectrolyte brush are long-ranged electrostatic interactions and short-ranged steric repulsion. When PS_{60}-b-PAA_{29} brush is immersed in water, the PAA chains become negatively charged. These charges are surrounded by cations and the spatial organizations of the charges introduce the Debye screening length $(1/k)$. The Debye screening length determines the excluded volume between the polymer chains and the conformational behavior of the chain.

PS_{60}-b-PAA_{29} is a good candidate for non-toxic coating because of several qualities that it possesses: it has been shown to be an affective bioactive implant specifically for use in the oral cavity (Jones et al, 2008). It is non-toxic in nature, its tunable charge density stemming from PAA being a weak polyelectrolyte, and it is inexpensive. The polystyrene block in PS-b-PAA is hydrophobic and it provides mechanical support when the block copolymer is attached to substrate's surface.

CHAPTER 3

METHODOLOGY

Deposition of the PS_{60}-*b*-PAA_{29} was accomplished by physical deposition using the Langmuir-Blodgett (LB) technique. Chemical deposition using atomic transfer rapid polymerization (ATRP) "grafting from" approach was also used to deposit PS-*b*-PAA. First, I will itemize the materials used followed by methodologies for the physical deposition and chemical deposition respectively.

<u>Materials</u>

Microscope glass slides (Fisherfinest premium microscope slides, plain. 3"x1" x 1mm) were purchased from Fisher Scientific. The glass slides were cut into small pieces of approximately 20 mm by 20 mm. Concentrated sulfuric acid (Lot # 064765), chloroform (Lot# 084860)), 1,4-dioxane (Lot# 070803, MW 88.11g/mol,), acetone(lot#097173), tetrahydrofuran (THF) (lot#107075), and toluene (Lot# 065981, MW92.14g/mol) were also purchased from Fisher Scientific, Fair Lawn, NJ, USA.

Hydrogen peroxide (35% wt, code 202460010), the free initiator, ethyl 2-bromoisobuthylrate (Br-iB) (lot#A016613101), and tert-butyl acrylate (tert-butyl) (Lot# A0287584) were purchased from Acros Organics, NJ, USA.

Ammonium hydroxide (Batch #185955 H, MW 35.05g/mol,), poly(acrylic acid) (PAA) (Lot# 10496MJ), poly(styrene)-block-poly(acrylic acid) (PS_{60}-*b*-PAA_{29}) (Product # 686794, Lot # MKBC0590, MW 8319g/mol,), N, N, N', N'', N'''-

pentamethyldiethylenetriamine (PMDETA) (Lot# S62866-419), and styrene (batch#MKBC0118) were purchased from Sigma-Aldrich, St. Louis, MO, USA. Polystyrene (Lot# 0001449235) was purchased from Fluka.

3-(Trimethoxysilylpropyl)-2-bromo-2-methylpropionate (TMSPBMB) (lot# SIT8397.0-5GM) was purchased from Gelest Inc, Morrisville, PA, USA, and Copper (I) bromide (Cu(I)Br) (lot# B01W008) was purchased from Alfa Aesar, Ward Hill, MA, USA.

Acridine orange (lot#766728) was purchased from Invitrogen molecular probes, Eugene, OR, USA. Deionized water (25°C, resistance of 18.2 MΩcm^{-1}), used as subphase, was obtained from Direct-Q UV 3 Millipore water purification system (Millipore, Eschborn, Germany). Surface pressure-area isotherms were obtained with Nima 312D mini trough (Nima Technology, UK, 7cm x 15cm). The trough was equipped with a 50 mm stroke dipper. Contact angle measurement was conducted with the ramé-hart model 500 advanced goniometer/tensiometer with DROPimage advanced software (rame-hart instrument co, Netcong, NJ, USA)

Physical deposition methodology

Poly (styrene)-block-poly(acrylic acid) (PS$_{60}$-*b*-PAA$_{29}$) was deposited using Langmuir-Blodgett deposition technique.

Surface pre-treatment

The preparation of modified glass slide is accomplished by first cleaning the microscope slide (substrate) in piranha solution (30:70 mixture of hydrogen

peroxide/concentrated sulfuric acid (30% H_2O_2)) (Rowe-Konopacki et al, 2007) resulting in the following reaction:

$$H_2SO_4 + 2H_2O_2 \rightarrow 2H_2O + O_2 + 2H^+ + SO_4^{2-} \xrightarrow{SiO_2} Si(OH)_4.$$
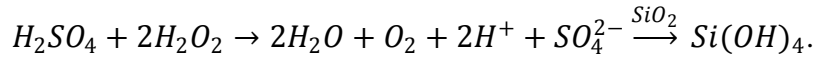
The solution was heated at 100°C for 2 hours and then rinsed with deionized water, followed by methanol.

Hydroxylation

In order to maximize the surface of the glass slide, the concentration of hydroxide ion on the surface was increased by soaking the cleaned glass slides in 30:70 mixture of hydrogen peroxide/deionized water (30% H_2O_2) (Jones et al, 2008) for 45 min at 70°C. After 45 min, 5mL of ammonium hydroxide was added.

$$2H_2O_2 + NH_4OH + SiO_2 \rightarrow H_2O + O_2 + NH_3 + Si(OH)_4$$
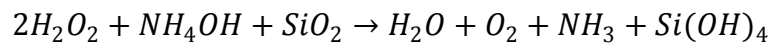
Once cooled, the substrates were rinsed with deionized water and then dried in methanol.

Application of "primer" to the surface of glass slides

Since we are interested in physically depositing the block copolymer on the surface of the glass slide, the LB film has to stick as soon as it touches the surface of the pre-treated glass slide. In order to promote "stickiness", polystyrene was deposited on the surface of the glass slide as follows: 11g/L of polystyrene was prepared by dissolving 275 mg of polystyrene in 25mL of chloroform. The solution was poured on the surface of glass slides in a beaker. The beaker was placed under the hood for 3 hours to 12 hours in order to allow complete evaporation of the

chloroform. The polystyrene coated glass produced is then placed in a vacuum oven (using pressure $\geq$ 25mmHg) and heated at 150°C for 3 days. This process will anneal polystyrene to the glass slides.

Once the annealing step was completed, the slides were washed with chloroform to remove excess polystyrene. The slides were allowed to sit under the hood for as long as necessary so the chloroform could evaporate.

Preparation of PS_{60}-b-PAA_{29}

The block copolymer was prepared by dissolving 25 mg of PS_{60}-b-PAA_{29} in 15mL of 1,4-dioxane. The solution was heated at 60°C for 2 days. Heating the solution allows all the PS_{60}-b-PAA_{29} powders to dissolve. 10 mL of toluene was added. The resulting solution was shaken to facilitate proper mixing.

Physical deposition of PS_{60}-b-PAA_{29}

Prior to the deposition of PS_{29}-b-$PAA_{60,}$ the self-assembly monolayer (SAM) of PS_{60}-b-PAA_{29} was prepared by spreading 90µL of PS_{60}-b-PAA_{29} at the air/water (A/W) interface. The monolayer was allowed to settle for 15-30 min before transferring the block copolymer to the surface of the polystyrene-modified glass.
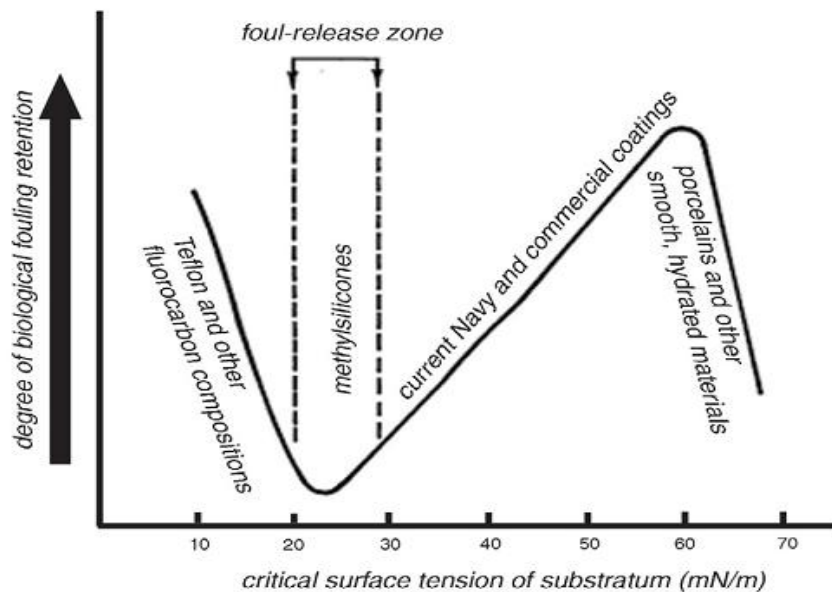
Figure 3.2: The Baier curve showing the degree of biofouling at specific surface pressures (Magin et al, 2010).

The deposition pressure was determined by looking at the Baier curve (Figure 3.2); a SAM deposited at a surface tension of 22-24mN/m will give a brush-modified surface with the lowest fouling (Magin, 2010).

Chemical deposition methodology

Surface pre-treatment

The preparation of modified glass slide was accomplished by first cleaning the microscope slide (substrate) in piranha solution (30:70 mixture of hydrogen peroxide/concentrated sulfuric acid (30% H_2O_2)) (Rowe-Konopacki et al, 2007) resulting in the following reaction:

$$H_2SO_4 + 2H_2O_2 \rightarrow 2H_2O + O_2 + 2H^+ + SO_4^{2-} \xrightarrow{SiO_2} Si(OH)_4$$
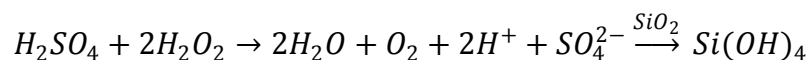
The solution was subjected to heat at 100°C for 2 hours and then rinsed with deionized water followed by methanol.

Hydroxylation

In order to maximize the surface of the glass slide, the concentration of hydroxide ion on the surface was increased by soaking the cleaned glass slides in 30:70 mixture of hydrogen peroxide/deionized water (30% H_2O_2) (Jones et al, 2008) for 45 minutes at 70°C. After 45min, 5mL of Ammonium Hydroxide was added.

$$2H_2O_2 + NH_4OH + SiO_2 \rightarrow H_2O + O_2 + NH_3 + Si(OH)_4$$
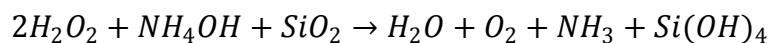
Once cooled, the substrates were rinsed with deionized water and then dried in methanol.

Silane modification

Place the freshly cleaned and hydroxylated glass slides into a 3-neck round bottom flask, add 270 mL of anhydrous toluene and install the reflux condenser. Close the openings with rubber septa. Flush with nitrogen for 30 minutes. Add 2.7 mL of 3-(Trimethoxysilylpropyl)-2-bromo-2-methylpropionate (TMSPBMB) and heat under reflux at 60°C for 4 hours. After 4 hours, stop the reaction and remove the silane modified glass slides. Wash with toluene, ethanol, and dry in a stream of nitrogen.

PAA modification of glass (Two 3-neck flasks were used for this reaction)

Flask 1: Silane modified glass slides were placed in the 3-neck flask and sealed with airtight rubber septa on the outer openings while the middle opening is fitted with a condenser that connects to a running tap water and the sink for discharge.

Flask 2: Acetone, Cu(I)Br, tert-butyl acrylate, and stir bar in the amount specified in Table 3.2 was added to the 3-neck flask and sealed with rubber septa. Place the flasks on two separate hot plates. Connect the flasks with cannula and insert needles into each flask to allow the escape of gas.

Figure 3.3: Experimental setup of the PS, PAA, and PS-*b*-PAA modification of glass substrate via ATRP.

Purge the assembly for 30 minutes with Nitrogen. Add PMDETA to flask 2 via a syringe and turn flask 2's hot plate to 90°C and stir for 10 minute. Turn off the gas and remove the pressure relief syringes.

Table 3.1: Reagents used in the ATRP grafting of poly(acrylic acid) brush.

250 mL total volume			
Number	Material	Concentration (mM)	Volume/Mass
1	Acetone	-	81.56mL
2	Cu(I)Br	15	537.9mg
3	Tert-Butyl	4.6	166.93mL
4	PMDETA	15	783.00µL
5	Br-iB	20	733.86 µL

Transfer the solution in flask 2 to flask 1 via the cannula (this may take 30 to 45 minutes). Once the transfer is complete, add the amount of free initiator (Br-iB) specified in Table 3.1 and remove the cannula. Turn hot plate 1 to 90°C and stir for the number of hours required for brush thickness.

Remove the slides and wash with THF. Place the slides in a bottle with screw cap, wrap parafilm around the cap and shake at moderate speed for 24 hours to remove unbounded tert-butyl acrylate. Sonicate for 30 minute and clean.

Hydrolysis of poly(tert-butyl acrylate) to poly(acrylic acid)

Poly(tert-butyl acrylate) modified glass slides were placed in a round bottom flask, 20 mL of dioxane and 3 mL of concentrated hydrochloric acid were added to the flask. The mixture was then heated under reflux at 100°C for 4 hours. Upon completion, the solution was allowed to cool, the glass slides were removed and cleaned with deionized water followed by methanol and dried in a stream of nitrogen.

28

PS ATRP modification of glass (Two 3-neck flasks were used for this reaction)

Surface pre-treatment and silane modification steps are the same as in the production of poly(acrylic acid) brushes.

Table 3.2: Reagents used in the ATRP reaction of poly(styrene) brush.

280 mL total volume			
Number	Material	Concentration (mM)	Volume/Mass
1	Anisole	-	153.08 mL
2	Cu(I)Br	12	481.6 mg
3	Styrene	4.6	125.12 mL
4	PMDETA	25	1.4616 mL
5	Br-iB	10	346.08 µL

There is no hydrolysis step for the fabrication of polystyrene brushes. Simply replace the reagents in Table 3.1 with the reagents in Table 3.2 for the PS ATRP modification of glass slides and follow the same steps under PAA ATRP modification of glass.

PS-*b*-PAA ATRP modification of glass

Follow the steps for the each block as outlined above.

CHAPTER 4

RESULTS AND DISCUSSIONS

Physical deposition of PS$_{60}$-b-PAA$_{29}$ Langmuir-Blodgett film

Surface treatment

In order to successfully transfer PS-*b*-PAA block copolymer to the surface of glass, pre-treatment of the glass substrate or any chosen surface is very critical and a determinant of the success of the polymer brush fabrication.

Currie et al, 2000 and many other research groups have spin-coated polystyrene on surfaces before physically adsorbing polymer films onto the substrate. When spin coating was tried in this project, the polystyrene delaminated from the substrate surface after being heated on a hot plate for about 10 minutes.

The method of Vos et al, 2008 proved better for making polystyrene surface for physisorption of PS$_{60}$-*b*-PAA$_{29}$ polymer brush. It involves pouring 11mg/mL of polystyrene solution prepared in chloroform onto the surface of cleaned glass slides and allowing the chloroform to evaporate under fume hood for about 12 hours to 24 hours. Polystyrene film formed on the surface of the glass but it was weakly bounded. In order for the polystyrene film to bind tightly, it was heated in vacuum oven for 72 hours at about 25 mmHg. Excess polystyrene was then washed off with chloroform. This caused thin film coating of polystyrene to be thermally bounded to the glass surface.

Upon deposition of PS_{60}-b-PAA_{29} on top of this modified glass at a preset surface pressure, the polystyrene block of the PS_{60}-b-PAA_{29} formed bond with polystyrene on the glass substrate; hence, polymer brush was formed.

Surface Activity of PS_{60}-b-PAA_{29} at air/water interface

Detail discussions of the theory of monolayer characterization using surface pressure-area isotherm and historic developments in monolayer science have been presented in Appendix B. The pKa of PAA is 4.5 (Gebhardt et al, 1983). The PS block of the PS_{60}-b-PAA_{29} block copolymer does not participate in the surface pressure as evidenced by a consistent increase in surface pressure in Figures 4.1 – 4.4 (Currie et al, 2000; Muller et al, 2008). The calculation of the volume required to form a PS_{60}-b-PAA_{29} monolayer and the area/molecule calculation of PS_{60}-b-PAA_{29} monolayer at fully opened and fully closed barrier positions can be found in Appendix C.

Before discussing the results, the specifics of the physical depositions of PS_{60}-b-PAA_{29} film are as follows: First, the solution of the polymer material is prepared as described under preparation of PS_{60}-b-PAA_{29} methodology, and then a monolayer is prepared by spreading the surfactant, from which the polymer brush is to be made, on the surface of the subphase in the Langmuir-Blodgett (LB) trough. The spreading solvent is then allowed to evaporate from the subphase surface. Next, the deposition surface pressure is then specified in the NIMA 7.8 software. Once the deposition surface pressure has been specified, the barriers of the LB trough (Figure 4.0) adjust themselves to maintain the pressure.
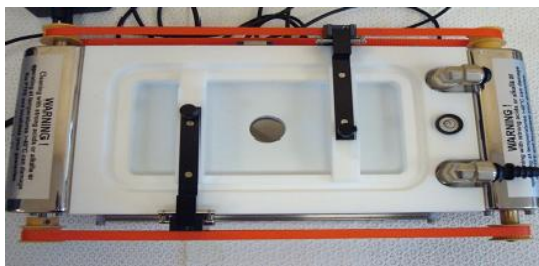
Figure 4.0: Langmuir-Blodgett trough equipped with two barriers and temperature control.

In salt-free deionized water, the hydrophilic block of the copolymer, PAA, became solvated and the protons in water complement the anions present on the PAA chains as much as possible. In essence, the chains of PAA 'diffuse' into water due to solvation.

In Figure 4.1, at 0°C and 15°C (deionized water), it was possible to pack the molecules very close to one another (as indicated by negligible pressure increase) as the barriers of the LB trough are closed. This is because the thermal (kinetic) energies of the molecules within the self-assembly monolayer (SAM) are low.
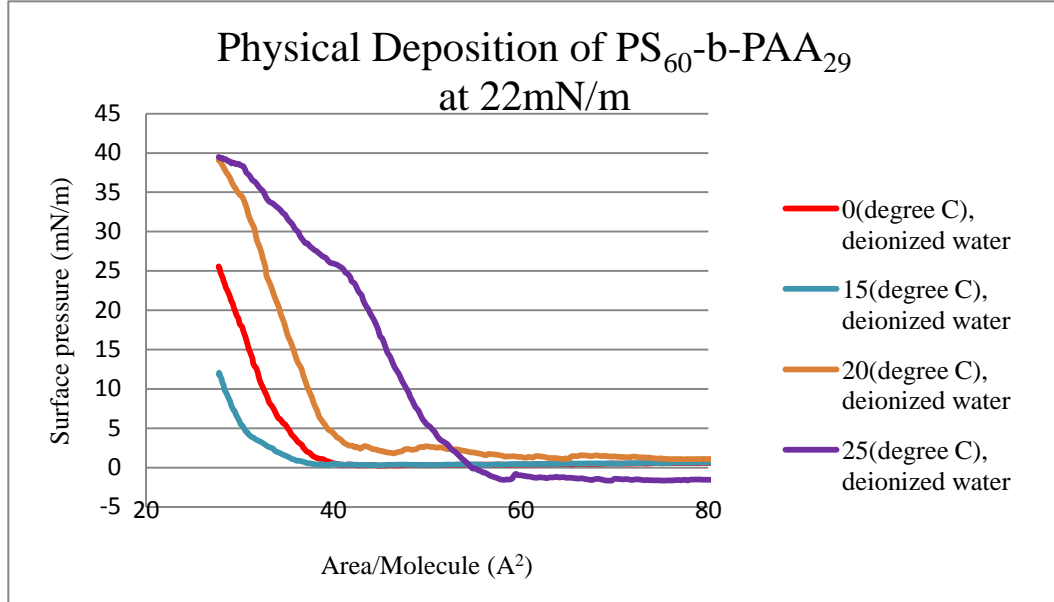
Figure 4.1: Surface pressure-area isotherm of the physical deposition of PS$_{60}$-*b*-PAA$_{29}$ Langmuir-Blodgett film at 0°C, 15°C, 20°C, and 25°C subphase temperatures prior to physisorption onto polystyrene modified glass surface. The subphase used was deionized water.

However, as an area/molecule of 42A^2-40A^2 was reached, a "phase change" (change from high state of disorderliness of polymer molecules (chains) to a more ordered state, that is, from 'gaseous state' to expanded monolayer phase) was observed indicating that the short-ranged steric force, long-ranged electrostatic repulsive force, and hydrophobic interactions among the polymer chains acted in concert as the molecules resisted packing too close to each other. So the pressure began to increase until the maximum pressure was observed.

The short-ranged steric repulsion can be expressed mathematically as follows (Evans et al, 1999):

$$\frac{F}{A} = (constant)\left(\frac{KT}{S^3}\right)\left[\left(\frac{2L}{h}\right)^{\frac{9}{4}} - \left(\frac{h}{2L}\right)^{\frac{3}{4}}\right] \quad h < 2L \quad \text{---------------------- (1)}$$

where F is force, A represents the area, KT represents the thermal energy (1.38 x 10^-23 J/K * temperature), L represents polymer brush thickness, and h is the distance of separation. While the long-ranged electrostatic force can be expressed according to the following mathematical representation (Evans et al, 1999):

$$\frac{F}{A} = 32(KT)^2 \frac{\varepsilon_r \varepsilon_0}{z^2 e^2} k^2 \Gamma_0^2 \exp(-kh) \qquad \text{----------------------- (2)}$$

where F is force, A represents the area, KT represents the thermal energy (1.38 x 10^-23 J/K * temperature), ε_r is a constant equal to 78.5, ε_o is the permittivity of empty space (8.85 x 10-12 C/Vm), e is the elementary charge, z represents ionic charge, Γ_o is the potential at a charged surface, $1/k$ is the Debye screening length, and h is distance of separation.

As temperature of the deionized water (subphase) increased to 20°C and 25°C respectively, the thermal energies of the surfactant molecules increased while the hydrophilic portion of the block copolymer remain ionized. Consequently, the degree of steric, electrostatic, and hydrophobic forces experienced by the molecules of the SAM were stronger and close packing of the molecules of the SAM could not be accomplished to the same degree experienced under 0°C and 15°C of deionized water. This phenomenon explains why the surface pressure started to rise at 60A^2 when the temperature of the deionized water subphase was increased to 20°C and 25°C.

Equations (1) and (2) predict that surface pressure is directly proportional to temperature (thermal energy); however, in Figure 4.1, the surface pressure-area isotherm indicates that the thermal energy at 15°C is lower than the thermal energy at 0°C leading to higher packing density at 15°C contrary to expectation. This unusual behavior presents a phenomenon that needs to be investigated further in order explain

what is happening within the surfactant molecules at air/water interface at 15°C.

In Figure 4.2, simulated sea water was used as the subphase while temperature and surface pressure were maintained at 20°C and 40mN/m respectively. The pH of the sea water was varied: 4.01 (acidic pH), 7.06 (neutral pH), and 9.96 (basic pH). The compositions of sea water are NaCl (58%), MgCl$_2$.6H$_2$O (26%), Na$_2$SO$_4$ (9.75%), CaCl$_2$ (2.765%), KCl (1.645%), NaHCO$_3$ (0.477%), KBr (0.238%), H$_3$BO$_3$ (0.071%), SrCl$_2$.6H$_2$O (0.095%), and NaF (0.007%). Sea water concentrations x ≤ 80mM, 80mM < x < 300mM, and x ≥ 300mM can be regarded as low, medium, and high concentrations respectively.
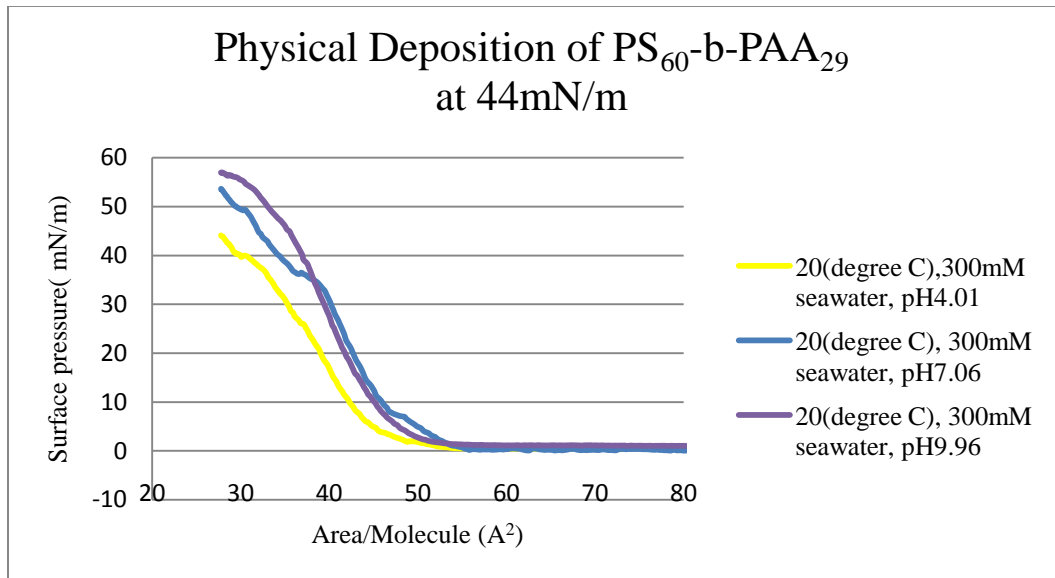
Figure 4.2: Surface pressure-area isotherm of the physical deposition of PS$_{60}$-*b*-PAA$_{29}$ film at 20°C subphase temperatures prior to physisorption onto PS modified glass surface. The subphase used was 300 mM sea water with pH adjusted to 4.01, 7.06, and 9.96 respectively.

Theoretical behavior models commonly used to describe polyelectrolyte brushes immersed in salt solutions are osmotic brush, salted brush, and neutral brush models.

Osmotic brush (OB) regime occurs when polyelectrolyte polymer brush immersed in water or salt solution swell due to the large osmotic pressure of the confined counterions (Lu et al, 2009). On the other hand, we have salted brush (SB) regime when the hydrogen ion (H^+) concentration in the polymer brush chains is approximately equal to that in the bulk solution due to dissociated protons in the brush undergoing constant exchange with salt ions from the bulk solution while maintaining electrical neutrality in the brush (Currie et al, 2000). Finally, neutral brush (NB) regime exists when the hydrogen ion (H^+) concentration inside and outside of the polymer brush is about the same and the electrostatic interactions are largely screened (Wu et al, 2007).

When sea water with concentration of 300 mM (high concentration) was used as the subphase, the cations in the sea water such as Na^+, Mg^{2+}, Ca^{2+}, K^+, and Sr^{2+} gathered around the negatively charged PAA chain in the salt solution and bind to those negative charges present on the surface of the chain. This phenomenon is called salt screening.

In a 300 mM - 500 mM sea water, the entire surface of a polymer brush becomes homogeneous (Witte et al, 2010). When the pH of the 300 mM sea water was maintained at 4.01, the PAA block of PS_{60}-b-PAA_{29} became neutral because the pH is less than the pKa of PAA (4.5), this means that in acidic pH up to 4.5, the -COOH groups of the PAA macromolecule exist in non-dissociated form (Chibowski

et al, 2006). Consequently, at pH below the pKa of PAA, we have NB regime. Also, there were minimal long-ranged electrostatic repulsive forces present within the molecules of the PAA group at pH 4.01 in the sea water; only the steric repulsive and hydrophobic forces were at play.

At pH 7.06 and pH 9.96 (values above the pKa of PAA), the –COOH group of the PAA chains of the block copolymer became dissociated, leading to equal H$^+$ concentration inside and outside the brush. This is because the degree of dissociation of the –COOH groups within the brush is also the same as that in the bulk solution. This results in SB regime. According to Currie et al, 2000, a mean-field model predicts the relationship for brush height and surface pressure using the following relationship: $H = N\sigma^{1/3}\left(\frac{\alpha_b^2}{\rho_s}\right)^{1/3}$ and $\pi = N\sigma^{5/3}\left(\frac{\alpha_b^2}{\rho_s}\right)^{2/3}$ ---------------------- (3) where H represents brush height, ρ_s is the salt concentration, α_b degree of proton dissociation in the bulk solution, and σ is the molecule (chain) per area.

According to equation 3, the increase in pH of the subphase should theoretically lead to increase in brush height and surface pressure once PS$_{60}$-b-PAA$_{29}$.

Surface pressure-Area isotherm shown in Figures 4.1 and 4.2 shows the maximum attainable surface pressure (MASP) upon the compression of the barriers of the LB trough. After physical deposition of the PS$_{60}$-b-PAA$_{29}$, the MASP in Figures 4.3 and 4.4 have reduced compared to the MASP in Figures 4.1 and 4.2. Hence, there was mass transfer (deposition) from the air/water interface to the polystyrene modified glass slides.
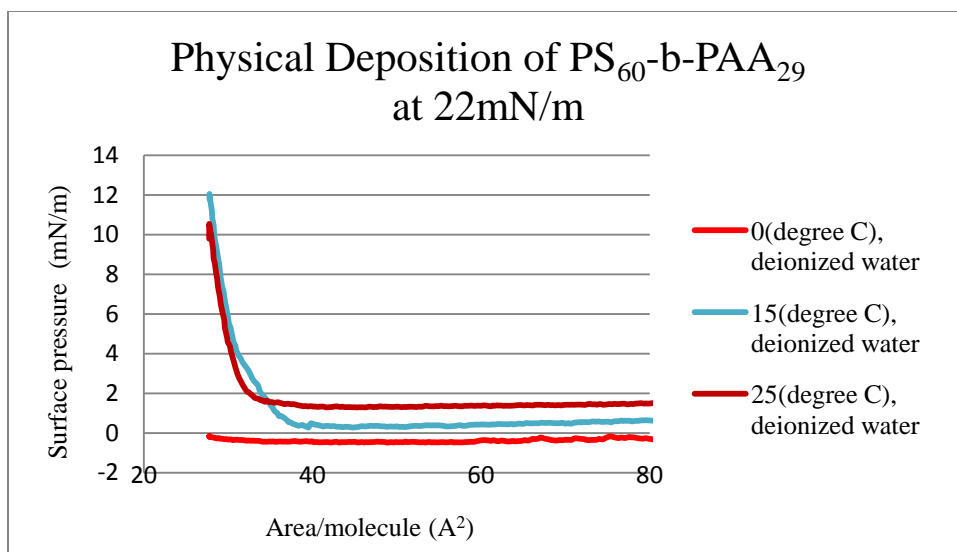
Figure 4.3: Surface pressure-area isotherm of the physical deposition of PS_{60}-*b*-PAA_{29} Langmuir-Blodgett film at 0^oC, 15^oC, and 25^oC subphase temperatures after physisorption onto polystyrene modified glass surface. The subphase used was deionized water.
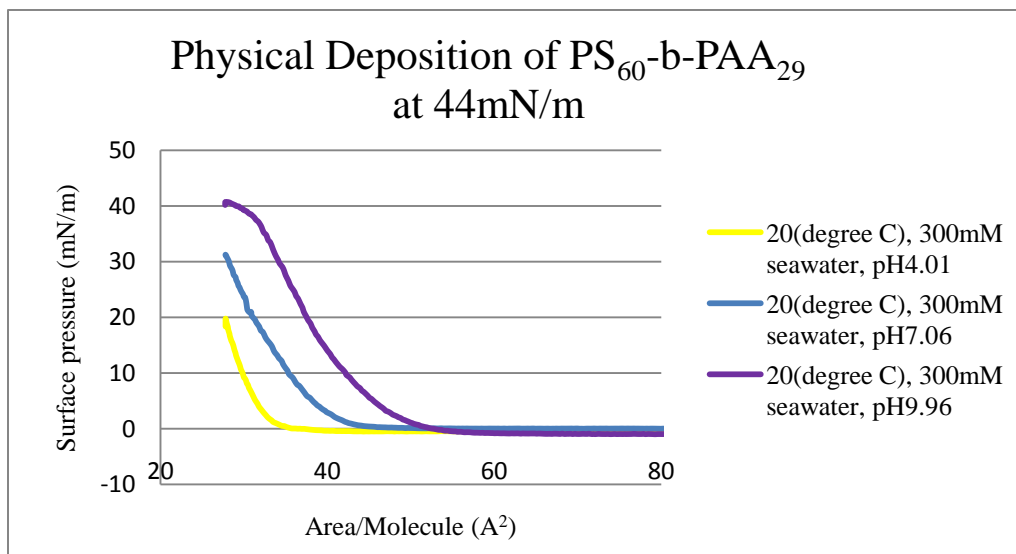
Figure 4.4: Surface pressure-area isotherm of the physical deposition of PS_{60}-*b*-PAA_{29} Langmuir-Blodgett film at 20^oC subphase temperatures after physisorption onto polystyrene modified glass surface. The subphase used was 300 mM sea water with pH adjusted to 4.01, 7.06, and 9.96 respectively.

Table 4.1: Transfer ratio of PS$_{60}$-b-PAA$_{29}$ from air/water and air/sea water interface. π is the surface pressure.

	Temp (^{o}C)	pH	Area/Molecule (A^2)	π (mN/m)	Transfer rate (%)
Before	15°C	-	27.76	39.49	91.52
After			27.73	3.35	
Before	25°C	-	27.76	47.38	79.34
After			27.75	9.79	
Before	20°C	4.01	27.77	44.08	58.42
After			27.78	18.33	
Before	20°C	7.06	27.78	53.67	42.02
After			27.78	31.12	
Before	20°C	9.96	27.77	57.00	29.5
After			27.75	40.14	

Table 4.1 presents the transfer ratio of PS$_{60}$-b-PAA$_{29}$ from air/water and air/sea water interface. The transfer ratio was calculated as follows:

$$Transfer\ ratio = \frac{\pi\ before\ deposition - \pi\ after\ deposition}{\pi\ before\ deposition} * 100\%$$

It can be seen that as temperature increased from 15°C to 25°C, the transfer ratio decreased. The same trend was observed when the pH was increased from 4.01 through 9.96 while holding the temperature and pressure constant at 20°C and 44mN/m respectively.

Confirmation of mass transfer in Figures 4.1- 4.4 and most importantly, the understanding that grafting density can be controlled by adjusting the pH of the subphase before deposition of any hydrophobic-block-hydrophilic block copolymer on to a hydrophobic surface, is the main advantage that physical deposition technique has over chemical deposition technique.

Contact angle measurements

Contact angle results from surface free energy between liquid and solid surfaces when surrounded by air or gases in general. Contact angle measurement can help one to understand wettability, affinity, adhesiveness, and repelling tendency of a surface. The mathematical expression for calculating contact angle is known as Young's Equation (Figure 4.5):

$$\gamma_{SV} = \gamma_{SL} + \gamma_{LV} Cos\theta,$$

$$\theta = Cos^{-1}\left(\frac{\gamma_{SV} - \gamma_{SL}}{\gamma_{SL}}\right)$$

where γ_{sv} represents the solid-vapor surface tension, γ_{sL} is the solid-liquid surface tension, and γ_{LV} is the liquid-vapor surface tension. Young's equation applies to homogenous and smooth surfaces.
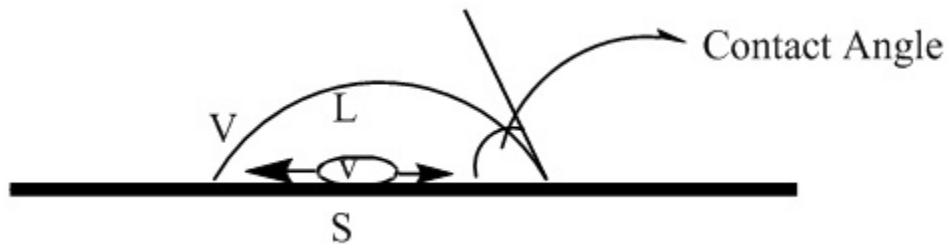
Figure 4.5: Contact angle schematic of water on a solid surface.

In order to estimate the contact angle on rough and heterogeneous surfaces, Wenzel and Cassie-Baxter relationships are commonly used (Figure 4.6). Wenzel regime occurs when the test liquid (deionized water) wets a surface such that there is a difference between the measured contact angle and the true contact angle; the

mathematical relationship that describes Wenzel regime is shown below (Genzer et al, 2006):

$$Cos\ (\theta_m) = R\ Cos\ (\theta_Y) = R\left(\frac{\gamma_{SV} - \gamma_{SL}}{\gamma_{SL}}\right)$$

where R is known as the roughness factor (ratio of true surface area and the projected surface area), θ_m is the Wenzel (apparent) contact angle on a rough surface and θ_Y is the Young's contact angle of the rough surface.

On the other hand, Cassie-Baxter wettability regime occurs when a surface that is made of small protrusions which cannot be filled by the deionized water (contact angle test liquid) are filled with air; the equation developed by Cassie and Baxter to model the contact angle on such rough surfaces is

$$Cos\ (\theta_C) = \sum f_i \cos(\theta_{Y_i})\ \text{(Konduru, 2010).}$$

where f_i is the fraction of each surface under liquid while θ_{Y_i} is the contact angle for the same surface.
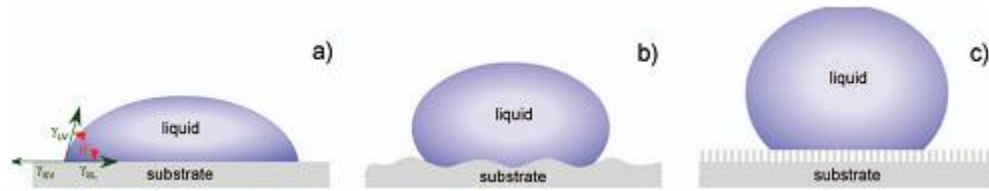
Figure 4.6: Liquid droplets spreading on a flat surface (a) and rough surfaces (b) and (c). The droplet is either in Wenzel regime (a) or the Cassie-Baxter regime (c) (Genzer et al, 2006).

In order to verify surface modification and understand the wetting behavior of the PS_{60}-b-PAA_{29} modified glass substrate, advancing contact angle measurement of the modified glass substrates were measured before and after physical deposition of

the LB film.

Advancing contact angle values were obtained with the ramé-hart model 500 advanced goniometer/tensiometer with DROPimage advanced software. Deionized water obtained from Direct-Q UV 3 Millipore water purification system was dropped on dry polymer brush modified glass slide. The water was allowed to spread for duration of 5 minutes or less. Averages of three readings were taken across different parts of the surface of each slide.

The advancing contact angle value of 48° for PAA and 97° for PS have been reported in the literatures (Boyes et al, 2004; Treat et al, 2006). In Figure 4.7, a clean and unmodified glass slide shows a contact angle of 51.2^o. Once pre-treated with polystyrene, the contact angle of the glass slides rose to values between 72.7^o and 91.4^o; this shows that the glass slide has been rendered hydrophobic.
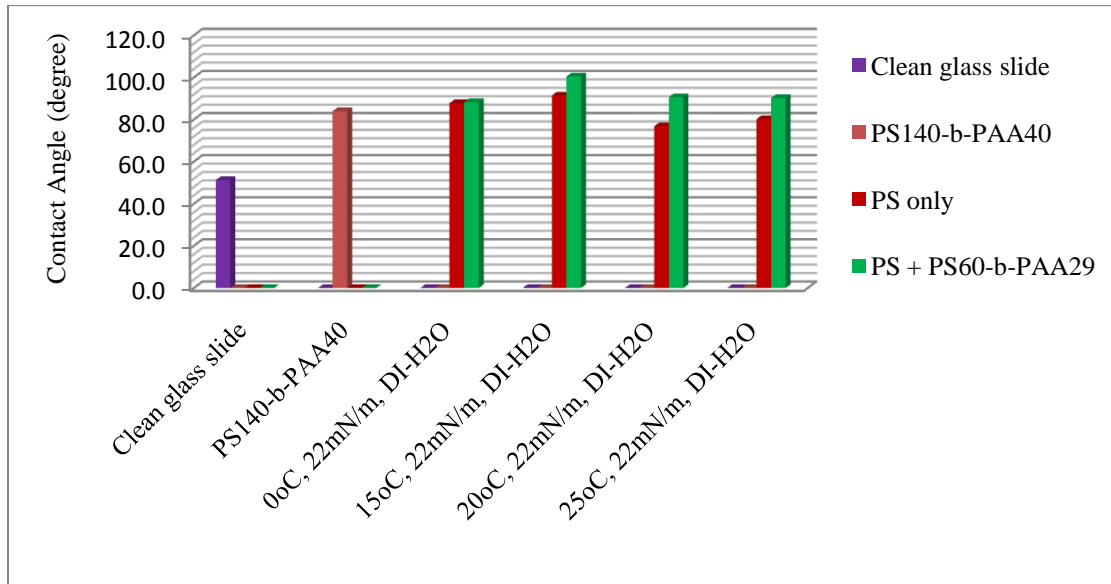
Figure 4.7: Advancing contact angle measurements of clean, unmodified microscope glass slide, microscope glass slides modified with polystyrene before and after deposition with PS_{60}-b-PAA_{29} respectively with changing temperature from 15^oC to 25^oC.

For temperatures between $0^{\circ}C$ and $25^{\circ}C$, when deionized water was used as the subphase, there was increase in contact angle after the physical deposition of the LB film. The meaning of this increase in contact angle is that the surface is more hydrophobic, probably due to one or more of the following reasons:

1. More polystyrene is present on the surface of the glass due to deposition of PS_{60}-*b*-PAA_{29} film. In other words, the non-wetting characteristic of the PS pre-treated glass substrate was enhanced after the deposition of PS_{60}-*b*-PAA_{29}.

2. Surface roughness of the substrate surface has increased because of the presence of nano-sized protrusions and nanoscale "hairy-looking" structures. Increase in contact angle may also be attributed to surface roughness after physical deposition of PS_{60}-*b*-PAA_{29} because when in-plane spaces are present on a polymer brush modified surface, upon dropping water droplet on such a surface, air pocket may be trapped in the spaces because of the unevenness of the surface, leading to the increase in contact angle. This wettability behavior may be modeled with Cassie-Baxter model (Figure 4.6c).

Figure 4.8 presents the advancing contact angle measurements of clean, unmodified microscope glass slide, microscope glass slides modified with polystyrene, and PS_{60}-*b*-PAA_{29} modified polystyrene pre-treated glass slides. In Figure 4.8, in addition to pH variation from 4.01 to 9.96, the subphase was changed from deionized water to 300 mM sea water (high concentration) while keeping the temperature and surface pressure constant at $20^{\circ}C$ and 40mN/m respectively. It can be noted that advancing contact angles have decreased after the physical deposition of the PS_{60}-*b*-PAA_{29}.

43
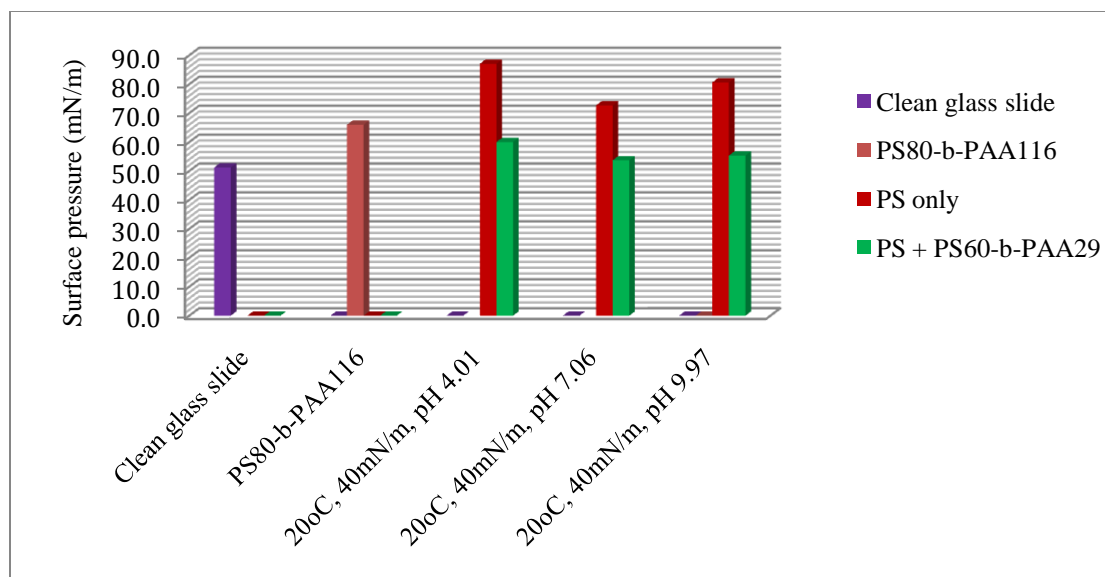
Figure 4.8: Advancing contact angle measurements of clean, unmodified microscope glass slide, microscope glass slides modified with polystyrene before and after deposition with PS_{60}-b-PAA_{29} respectively with pH variation from 4.1 to 9.96.

The decrease in contact angle could be attributed to:

1. Increase in grafting density of PS_{60}-b-PAA_{29} brush on the substrate surface – more PAA chain per area would cause decrease in contact angle because PAA is hydrophobic, thus giving contact angle values that are close to the literature value of PAA (48°). Visual inspection of the brush made at 40 mN/m surface pressure indeed indicated a higher mass transfer of PS_{60}-b-PAA_{29} and greater grafting density when compared to the brush made at 22 mN/m surface pressure; the brushes at pH 4 has lower grafting density and exercise slightly lower wettability than the brushes at pH 7 and 10.

2. A very homogeneous surface with little or no in-plane space. It is possible to describe the brush made at pH 7 and 10 (using 300 mM sea water, 40 mN/m surface pressure) with Wenzel model as shown in Figure 4.6b.

Although, it has been indicated on the Baier curve that foul-release coating can be achieved when a surface has a surface energy of 22 mN/m-24 mN/m, additional factors such as nanoscale or microscale roughness can affect fouling (Carman et al, 2006).

In this nanoscale fabrication work, we suspect that contact angle variations can be attributed to nanoscale roughness of the polymer brush modified surface. Although at this moment, we cannot directly determine how nanoscale roughness affected the contact angles but it is safe to assume that the contact angle measurement did not only relate to the degree of wettability of the surfaces but it also revealed the presence of nanoscale roughness via grafting density variation that is absent from ATRP deposition technique.

UV-vis transmittance

UV-vis spectroscopy is a technique in which the ability of electron to be excited and move between energy levels is utilized. These energy levels have direct correlation to the molecular orbital of the systems. Specifically, UV-vis spectroscopy takes advantage of electronic transitions involving π orbitals and lone pair electrons to identify conjugated systems which have stronger absorptions. The wavelength of ultraviolet light is 200 nm - 400 nm while that of visible light is 400 nm - 800 nm. Detail discussion of this technique has been carried out in Appendix B.

It can be seen in Figure 4.9 that there are three regions of transmittance: **Region 1** comprises of clean glass slide and the polymer brushes prepared at 20°C and 25°C using deionized water as the subphase. 100% of the UV-vis light was

transmitted in this region between wavelengths of 350 nm to 800 nm.

In **region 2,** the brushes at 0°C and 15°C (both with deionized water subphase) and the polymer brush at pH 9.96 (20°C, 300mM sea water subphase) all have transmittances of between 74 % - 98 % over a wavelength range of 350 nm to 800 nm. Finally, **region 3** comprises of polymer brushes fabricated at 15°C (deionized water subphase), brushes made at pH 4.01 (20°C, 300 mM sea water subphase), and the brushes prepared at pH 7.06 (20°C, 300 mM sea water subphase) over a wavelength range of 350 nm to 800 nm.

In sum, the UV-vis transmittance measurements suggest that the PS$_{60}$-*b*-PAA$_{29}$ polymer brush modified surfaces are semi-transparent, which is important for applications in lenses or windows.
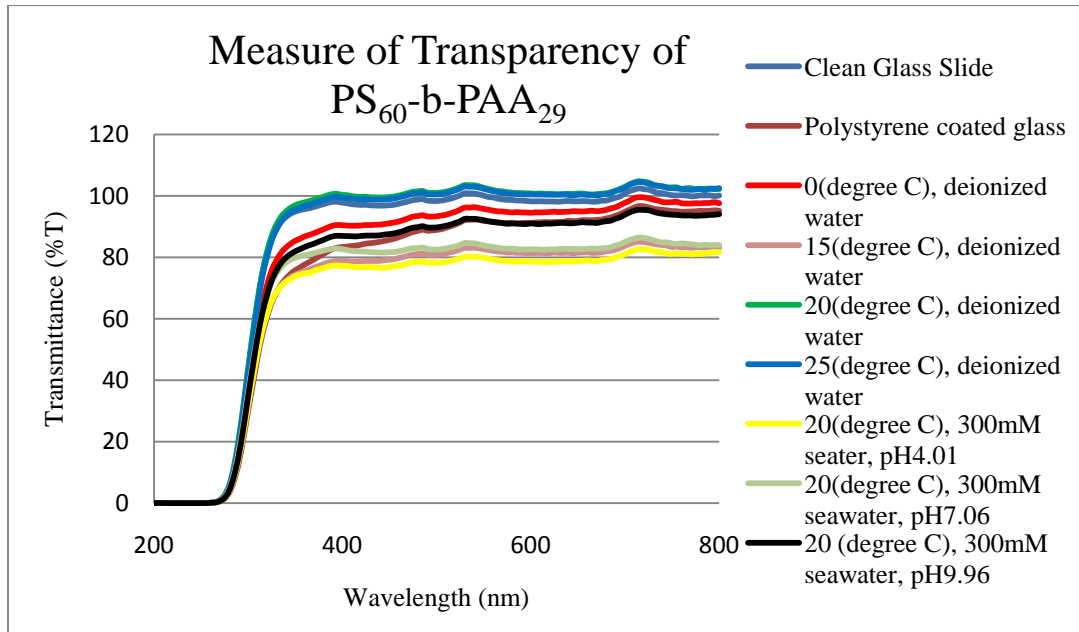
Figure 4.9: Transmittance of UV-vis light through PS$_{60}$-*b*-PAA$_{29}$ modified glass slides. Subphase temperature and pH, as well as, deposition pressure were varied to understand the effect those changes on the brush-modified surface.

Fluorescence imaging studies

Fluorescence occurs when a material emits light within nanoseconds or femtoseconds upon absorption of light with short wavelength (Lichtman et al, 2005). Not all the absorbed lights are emitted but the emitted light (known as fluorescence) by the material has longer wavelength than the incident light. Emitted fluorescence is then collected by the objective of the microscope and sent to the detector. In order to observe fluorescence, fluorophore is needed to "label" the sample molecules. Fluorophores are molecules or compounds that possess fluorescence properties. Details of the operation and principles of fluorescence microscopy have been discussed by Muller, 2006 and Lichtman et al, 2005.

The fluorophore used in this work is acridine orange. It binds to the carboxyl group of the PAA in PS-*b*-PAA. The fluorophore solution was prepared by dissolving acridine orange in deionized water to make 1 mg/mL solution (probably too concentrated as shown by the fluorescence images below). The solution was poured on the polymer brush and allowed to stain the sample for approximately 30 minutes. The samples were washed with deionized water after staining. Upon the completion of fluorophore rinsing, the samples were placed on the fluorescence microscope and images were obtained using confocal microscope at magnification of 200X – 400X. Figures 4.10 - 4.13 shown below presents the surveys of the surfaces of glass slides as observed under fluorescence microscope. Figure 4.10A shows the surface of clean glass slide that was not modified while Figure 4.10B is the fluorescence micrograph of polystyrene modified glass slide; patterns could be seen across the surface the glass slide. It should be noted that polystyrene does not fluoresce with acridine orange

because it does not have any molecular group that binds to acridine orange; however, the patterns that are seen most likely came from the polystyrene that were deposited on the glass slides because there are no stripes present on the clean glass slide' fluorescence image.
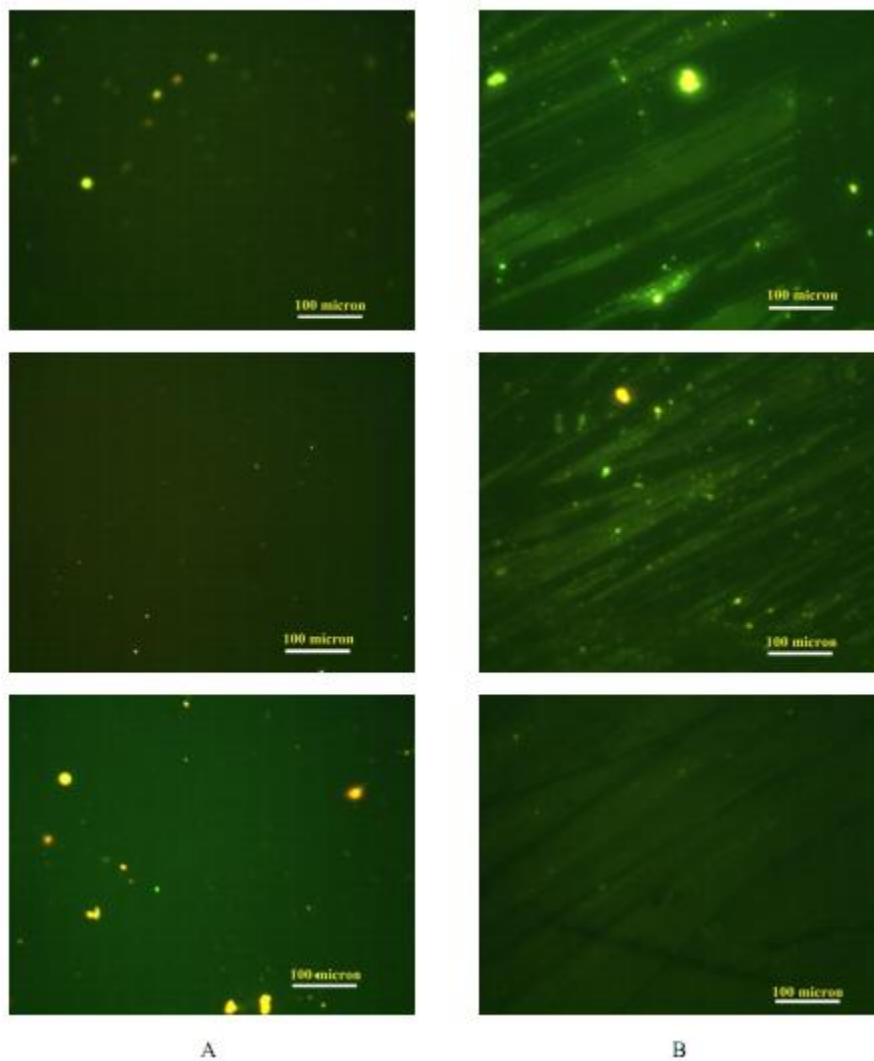
Figure 4.10: Fluorescence micrograph of (A) clean glass slides (control) and (B) polystyrene modified glass slides prepared by pouring PS solution on glass and annealing at 150°C for 3 days.
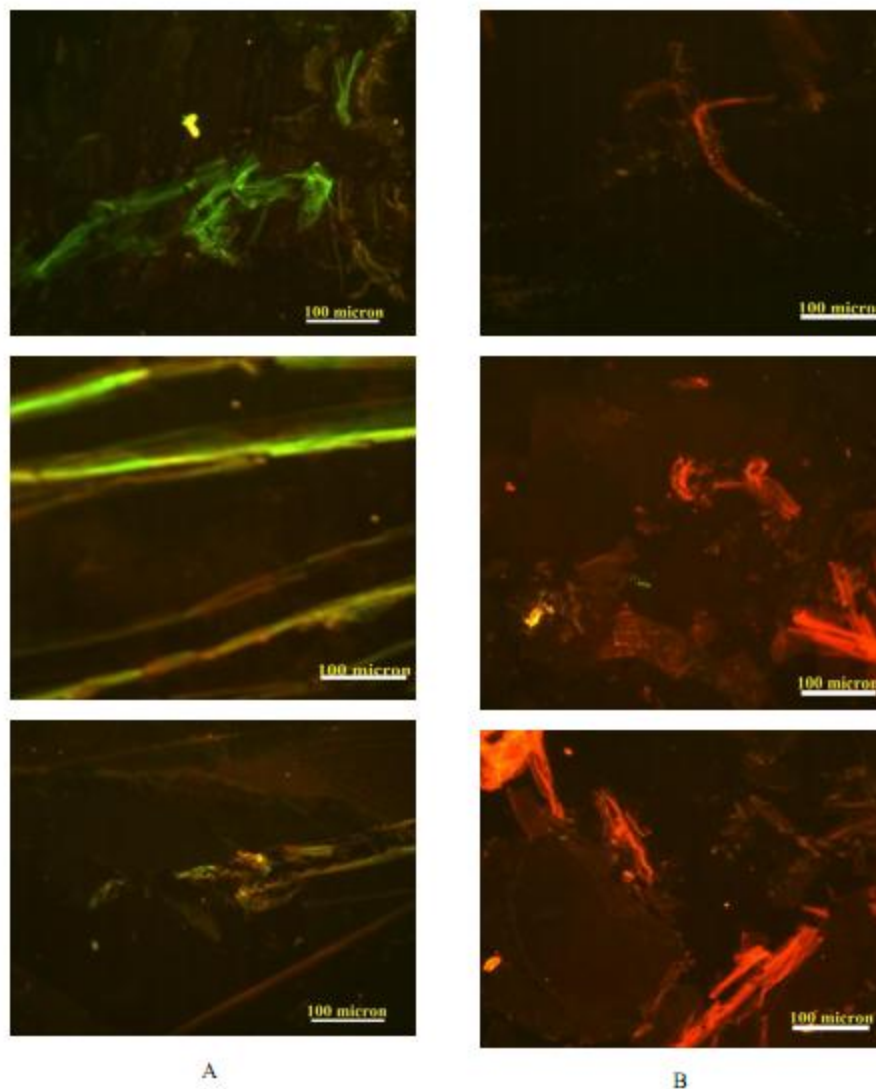
Figure 4.11: Fluorescence micrograph of (A) dry PS_{60}-b-PAA_{29} brush prepared at $\pi = 22$ mN/m using deionized water as subphase (T = 20°C) and (B) dry PS_{29}-b-PAA_{60} brush prepared at $\pi = 40$ mN/m using 300 mM sea water as subphase (T = 20°C, pH = 9.96).

The fluorescence micrographs presented in Figure 4.11 are (A) dry PS_{60}-b-PAA_{29} brush prepared at $\pi = 22$ mN/m using deionized water as subphase (T = 20°C) and (B) dry PS_{29}-b-PAA_{60} brush prepared at $\pi = 40$ mN/m using 300 mM sea water as subphase (T = 20°C, pH = 9.96). The non-hydrated brushes prepared at 0°C, 15°C,

49

and 25°C are not shown. In addition, images are not shown for non-hydrated brush prepared at $\pi = 40$ mN/m using 300 mM sea water as subphase (T = 20°C, pH = 4.01 and pH 7.06). So, in Figure 4.11, the non-hydrated brushes organized into long strips or coils of polymer mosaic probably due to collapse of the PAA chains.
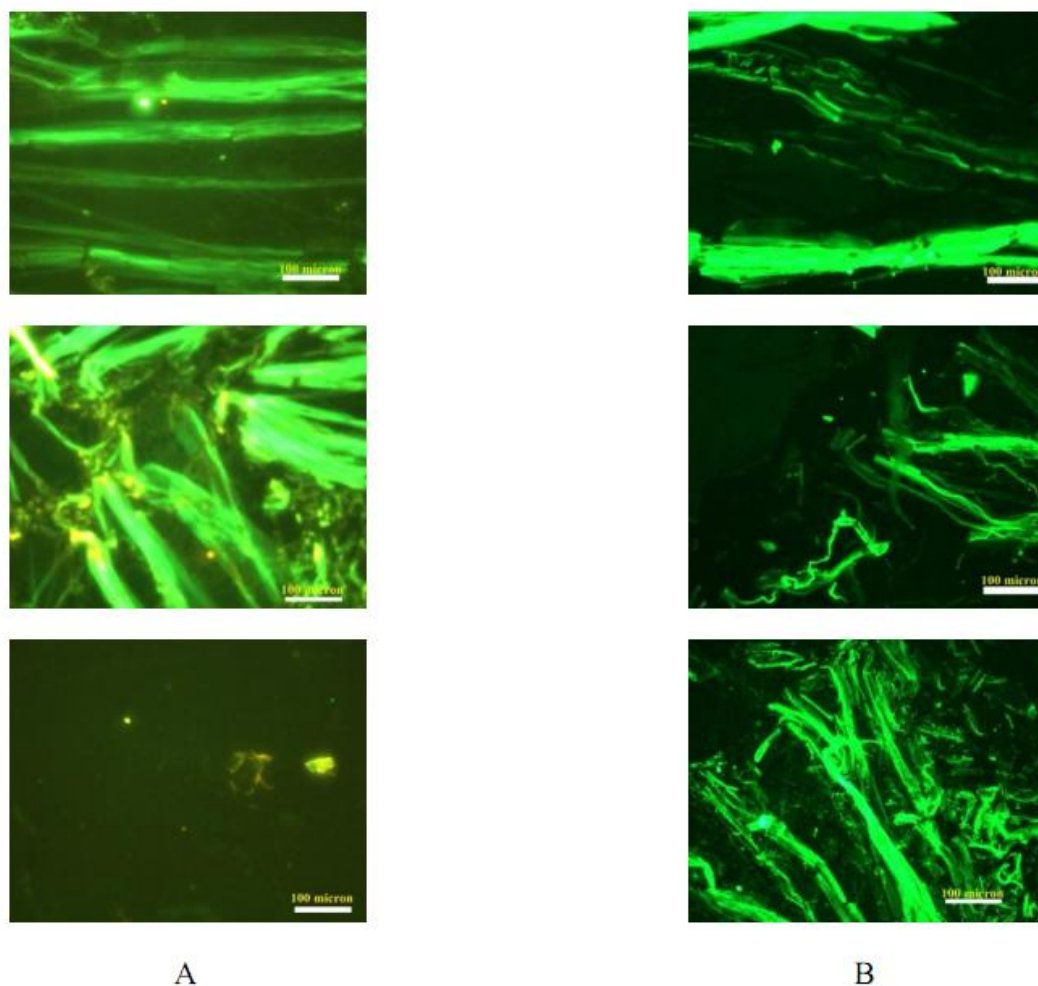
Figure 4.12: Fluorescence micrograph of (A) hydrated PS_{60}-b-PAA_{29} brush prepared at $\pi = 22$ mN/m using deionized water as subphase (T = 20°C) and (B) hydrated PS_{29}-b-PAA_{60} brush prepared at $\pi = 22$ mN/m using deionized water as subphase (T = 25°C).

However, when the brushes were hydrated as shown in Figure 4.12, it reveals that the PAA blocks of the copolymer became extended and swollen. It can be seen that the density of the brushes increased due to wetting (evidence of hydrophilic nature of PAA).

In Figure 4.13, the surface pressure, subphase, and pH were changed in order to study the behaviors of the polymer brush. It can be seen that as the deposition pressure was changed from 22 mN/m, the surface energy of the resulting brush and surface morphology of the brush produced also changed.
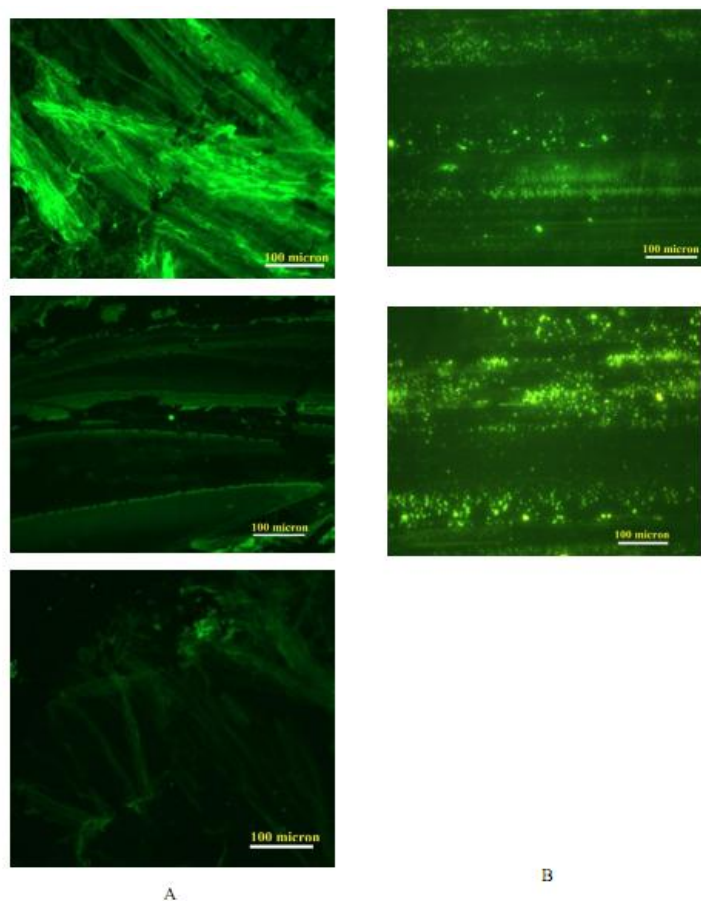
Figure 4.13: Fluorescence micrograph of (A) hydrated PS_{60}-b-PAA_{29} brush prepared at $\pi = 40$ mN/m using 300 mM sea water as subphase (T = 20°C, pH = 4.01) and (B) hydrated PS_{29}-b-PAA_{60} brush prepared at $\pi = 40$ mN/m using 300 mM sea water as subphase (T = 20°C, pH = 9.96).

At acidic pH (4.01), the PAA blocks of the PS_{60}-b-PAA_{29} are neutral because pH 4.01 is below the pKa value of PAA. We can see horizontally positioned, elongated, and leaf-like appearance of PS_{60}-b-PAA_{29} brush on the glass surface at pH 4.01. At basic pH (9.97), the PAA blocks of the PS_{60}-b-PAA_{29} become ionized (the carboxylic groups of the PAA chain ionizes) and acquire negative charges, the acquisition of charges results in steric and electrostatic repulsions. It can also be seen that the brush look like dots instead of strand-like appearance that was observed when the film was dry.

This dot-like appearance proved that the PAA blocks have stretched. This may have resulted in increase brush thickness. Also, Xu et al, 2006 provided evidence that at pH above the pKa of PAA (4.5), the PAA chains stretch as the pH increases. So, when the pH was raised to values above the pKa, brush density thickness increased.

Atomic force microscopic (AFM) analysis

AFM is a good analytical tool for characterization of polymer brush surfaces. It can be used to study surface morphological and topographical features, measure thickness, and investigate mechanical properties of polymer brush modified surfaces.

AFM takes surface measurement by scanning the tip of the cantilever on a surface resulting in an attractive or a repulsive interplay with the surface. As a result of these interactions, the tip attached to a cantilever experiences a force that causes the cantilever to bend. A laser beam off the cantilever detects the deflection of the cantilever causing the degree of the laser beam to be translated to image in terms of height or topography (Kolasinski, 2008). More details on AFM can be found in

Appendix B.

The AFM images presented in presented in Figures 4.14 and 4.15 were acquired by our collaborator, Dr. John Torres, at the Naval Undersea Warfare Center (NUWC). These images are preliminary in nature and are only meant to give a qualitative idea of the surface morphological features of the physically deposited PS_{60}-b-PAA_{29} brushes. Therefore we cannot deduce quantitative information such as brush thickness and root-mean-square roughness from these images because the scale bars are missing. The samples were hydrate before AFM images were acquired.

Evidence of surface pre-treatment could be seen on the polystyrene modified glass slides in Figures 4.14A and 4.15A. The presence of protrusions, stripes, and bumps is consistent with the features seen in Figure 4.10B (fluorescence image) and it clearly shows that polystyrene was successfully deposited on the surface of glass slides. The AFM image of clean glass slide is not shown but it was flat with the absence of all the features seen on Figure 4.14A.

In Figure 14B - D, PS_{60}-b-PAA_{29} film was transferred from air/water interface at π=22mN/m (subphase T=0°C, Figure 4.14B) π=22mN/m (subphase T=20°C, Figure C), and π=22mN/m, (subphase T=25°C, Figure D). They all show unique surface morphologies. In addition, phase separations (characterized by dot-like appearances of PAA protrusions on top of polystyrene background or surface micelles) could be seen in all the AFM images.
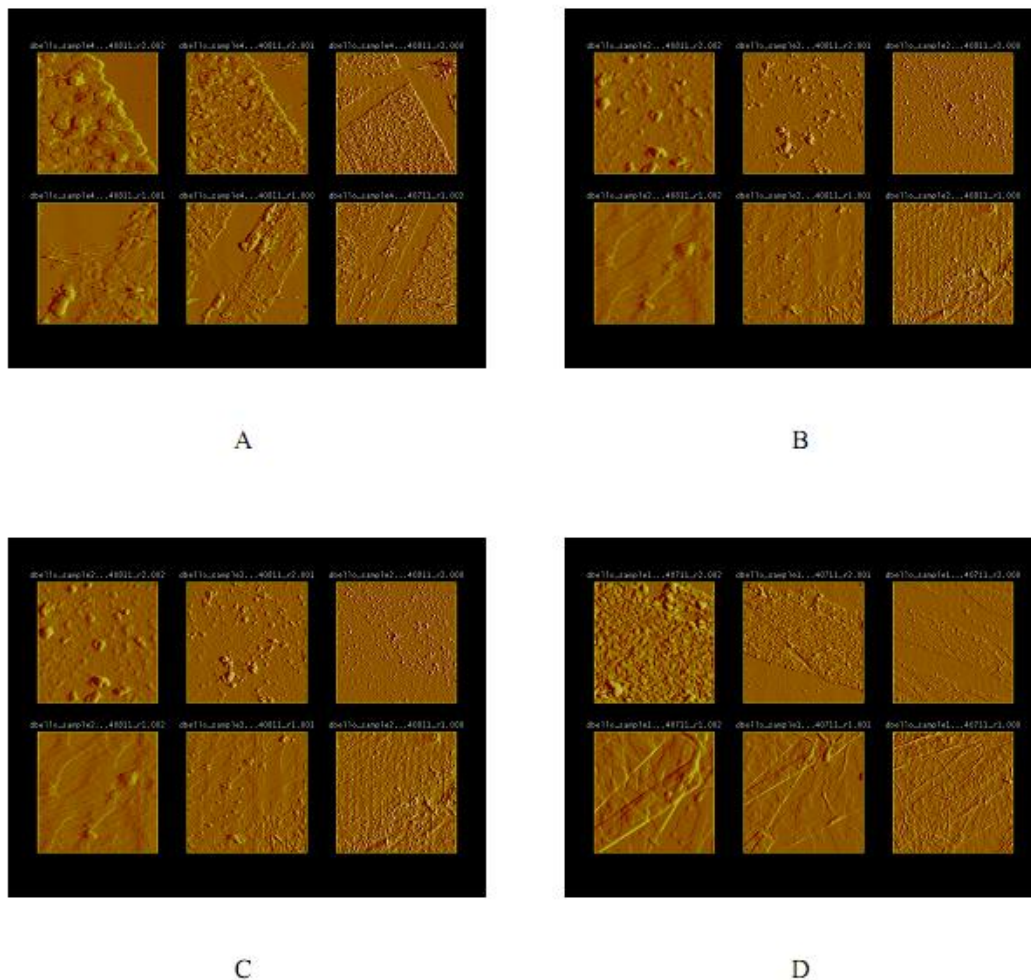
Figure 4.14: Atomic force microscope images of (A) polystyrene modified glass slides prepared by pouring PS solution on glass and annealing at 150°C for 3 days, PS_{60}-b-PAA_{29} transferred from air/water interface at (B) π=22mN/m, T=0°C, (C) π=22mN/m T=20°C, and (D) π=22mN/m, T=25°C. Each column from left to right is 5 μm x 5 μm, 10 μm x 10 μm, and 30 μm x 30 μm in size.

In Figure 4.15B – D the temperature was kept constant at 20°C, deposition surface pressure was change to 40 mN/m, subphase was changed from deionized water to sea water, and the pHs were varied; pH 4.01, pH 7.06, and pH 9.96. The effects of the changes are:
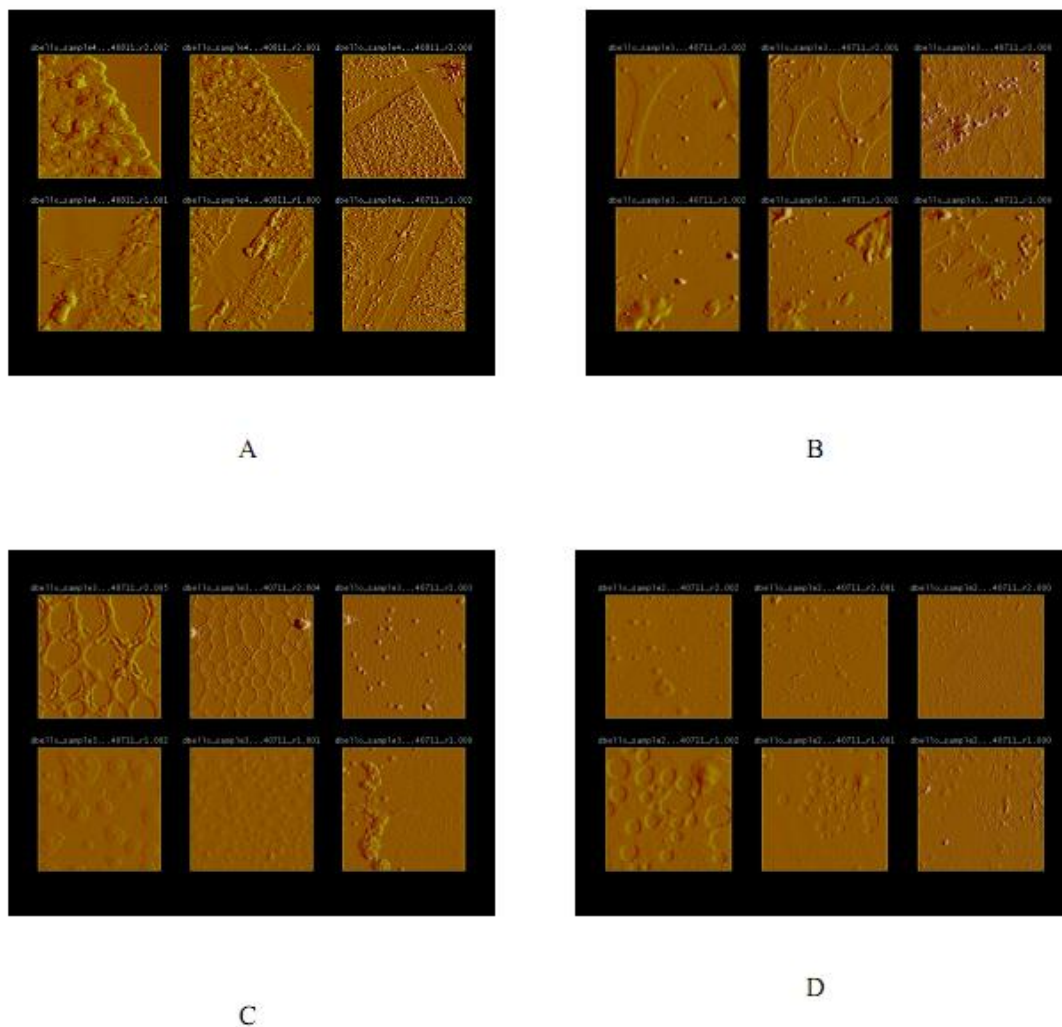
Figure 4.15: Atomic force microscope images of (A) polystyrene modified glass slides prepared by pouring PS solution on glass and annealing at 150°C for 3 days, PS_{60}-b-PAA_{29} transferred from air/sea water interface at (B) π=40mN/m (T=20°C, pH4.01), (C) π=40mN/m (T=20°C, pH7.06), and (D) π=40mN/m (T=20°C, pH9.96). Each column from left to right is 5 μm x 5 μm, 10 μm x 10 μm, and 30 μm x 30 μm in size.

1. Figure 4.15B - change in grafting density, reduction of surface roughness, and characteristic surface micelle formation. This is consistent with fluorescence image in Figure 4.13A.

2. Figure 4.15C - in addition to charge screening and change in surface density, there are aggressive topographic formations of PS_{60}-b-PAA_{29} brush on the glass

surfaces caused by bridging of the surface micelles in some cases and micelle island in other cases. Fluorescence imaging of the pH 7.06 is not shown.

3. Figure 4.15D – the dot-like formation in Figure 4.13B (fluorescence image) are seen here as 'hills and valleys' of surface micelles which indicate the effect of charge screening.

It is not clear at this moment whether the topographic formations and surface micelles seen in all the cases of pH changes in Figure 4.14 and Figure 4.15 will enhance or worsen the anti-biofouling properties of the modified surface. The effect of the topographic formations and surface micelles will be observed once the antifouling studies are conducted.

Although, quantitative AFM work was not done to determine the thickness of the transferred monolayer; however, the length of the PS and PAA monomers have been estimated below:

Length of polystyrene monomers

$$M_n = 6213, \quad \#of\ monomer = 60, \quad ccc\ bond = 0.253$$

$$Persistent\ length = 0.253(60)^{1/2} = 1.96\ nm$$

$$fully\ extended\ length = 0.253 * 60 = 15.18\ nm$$

Length of poly(acrylic acid) monomers

$$M_n = 2106, \quad \#of\ monomer = 29, \quad ccc\ bond = 0.3$$

$$Persistent\ length = 0.3(29)^{1/2} = 1.62\ nm$$

$$fully\ extended\ length = 0.3 * 29 = 8.7\ nm$$

$$Total\ length = fully\ ext\ length\ of\ PS + fully\ ext\ length\ of\ PAA = 23.88\ nm$$

Therefore, the estimated thickness of the PS_{60}-b-PAA_{29} brush is 23.88 nm.

Chemical Deposition of PS$_{60}$-b-PAA$_{29}$ Langmuir-Blodgett film

In an effort to compare the anti-biofouling efficiency of chemically and physically deposited PS-*b*-PAA films, ATRP reaction was conducted. Surface characterizations are hereby discussed first.

Contact angle measurements

Figure 4.16 shown below is the advancing contact angle measurements of the chemically deposited polymers. The contact angle values obtained for unmodified glass slide is valid because glass should be hydrophilic. Glass treated with ammonium hydroxide, in order to maximize the surface area of the glass that is available for reaction, is more hydrophilic than non-hydroxylated glass as expected.
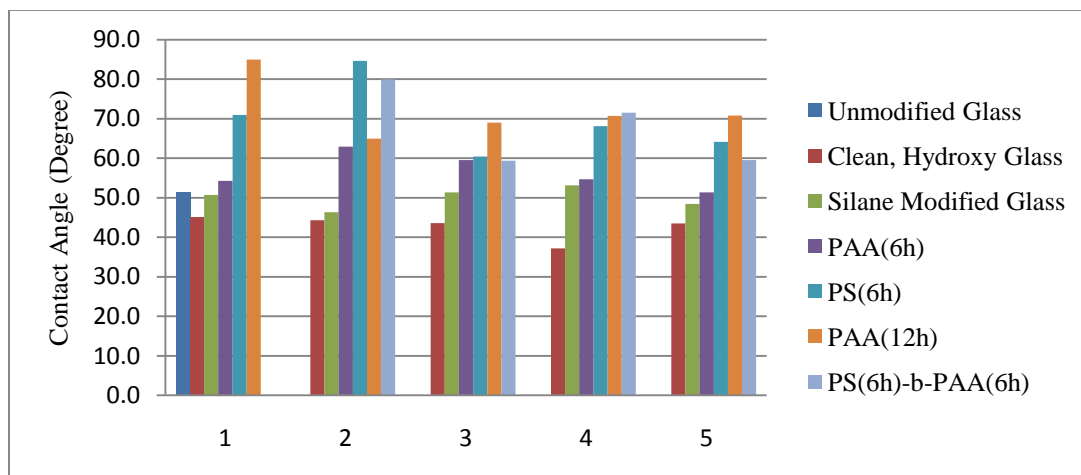
Figure 4.16: Advancing contact angle measurements of clean and unmodified glass slide, hydroxylated glass slides, silane modified glass slides, polystyrene modified glass slides (6 hrs ATRP), and poly(acrylic acid) glass slides (6 hrs and 12 hrs ATRP).

However, after silane modification, the glass slides became hydrophobic. This is by design because we intended to tether the hydrophobic end of the antifouling polymer on to the glass substrate.

For polystyrene, after 6 hours of ATRP reaction, advancing contact angle measurements in Figures 4.16 and 4.17 shows that there deposition of the polymer onto the surface of silane treated glass. The contact angle shows an indication of hydrophobicity. The literature values of advancing contact angle for polystyrene varies; Drechsler et al, 2005 and Sohn et al, 2011 reported the advancing contact angle of spin coated polystyrene of 91.7^{o} and 97.2^{o} respectively.
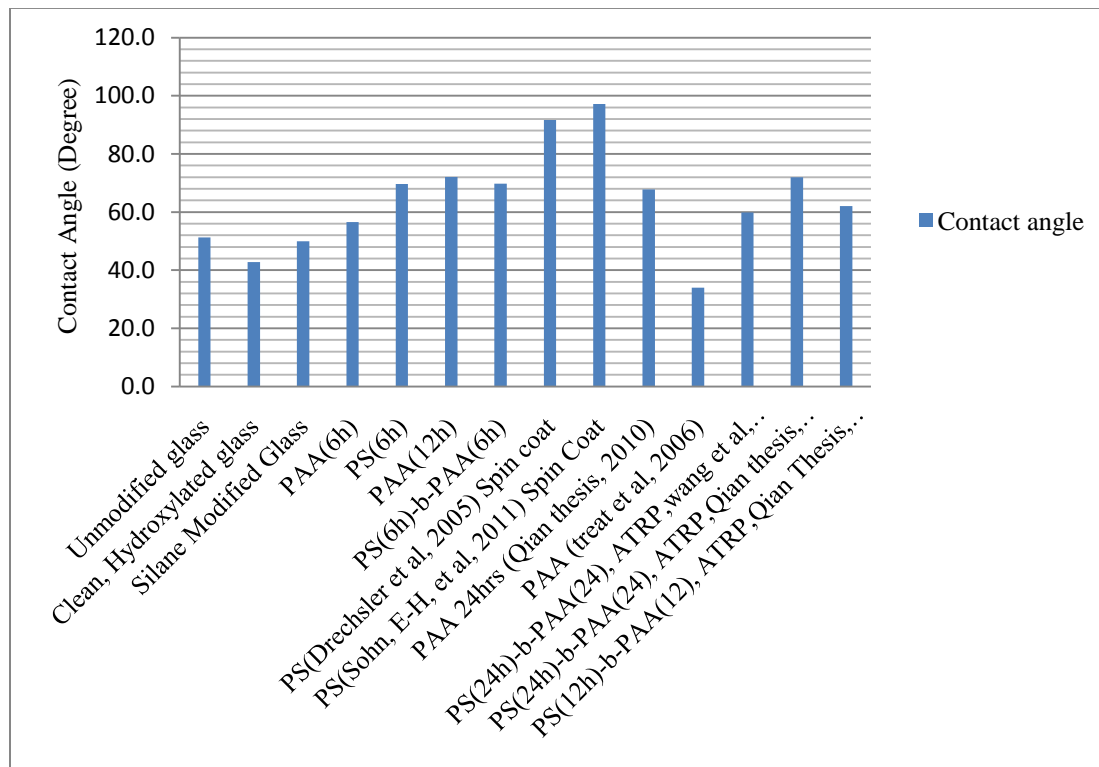
Figure 4.17: Average Advancing contact angle measurements of clean and unmodified glass slide, hydroxylated glass slides, silane modified glass slides, polystyrene modified glass slides (6 hrs ATRP), and poly(acrylic acid) glass slides (6 hrs and 12 hrs ATRP).

Most importantly, the grafting from ATRP reaction yielded a polystyrene modified hydrophobic surface.

PAA was grafted from the surface for 6 hours and 12 hours by ATRP. The advancing contact angle measurements are 56.5^{o} for the 6 hours brush and 72.1^{o} for the 12 hours brush (Figures 4.15 and 4.16). This was expected because the chain length and grafting density of the 12 hours PAA brush is supposed to be higher than that of 6 hours PAA brush because with time, the chain length of the brush should increase. This is an indication that the surface was modified. Treat et al, 2006, reported an advancing contact angle of 34.0^{o} for PAA but Ni, 2010 (MS Thesis) reported a higher contact angle of 67.8^{o} after 24 hours of grafting. Overall, the PAA contact angle values are high compared to the value obtained by (Treat et al, 2006), this could be due to incomplete hydrolysis of the poly(tert-butyl acrylate) to poly(acrylic acid). It has been shown by Ni, 2010 (MS Thesis) that poly(tert-butyl acrylate) does not completely hydrolyze in 4 hours; 8 hours was better.

The last set of brushes that were grown with ATRP was PS-*b*-PAA brushes. Advancing contact angle measured was 69.7^{o}. PS-*b*-PAA advancing contact angle measured by Wang et al, 2006 (24 hours) and Ni, 2010 (MS Thesis) (12 hours and 24 hours) were 59.8^{o}, 62.0^{o}, and 72° respectively. Although the values of contact angles obtained at 12 hours and 24 hours are close but disparities still exist in these contact angle values.

Uv-vis transmittance

Brushes fabricated by ATRP were tested for transparency by UV-vis spectroscopy and Figure 4.18 shows that chemically modified surface by ATRP also transmitted all the lights that passed through them as was the case with physical deposition surfaces in Figure 4.9.
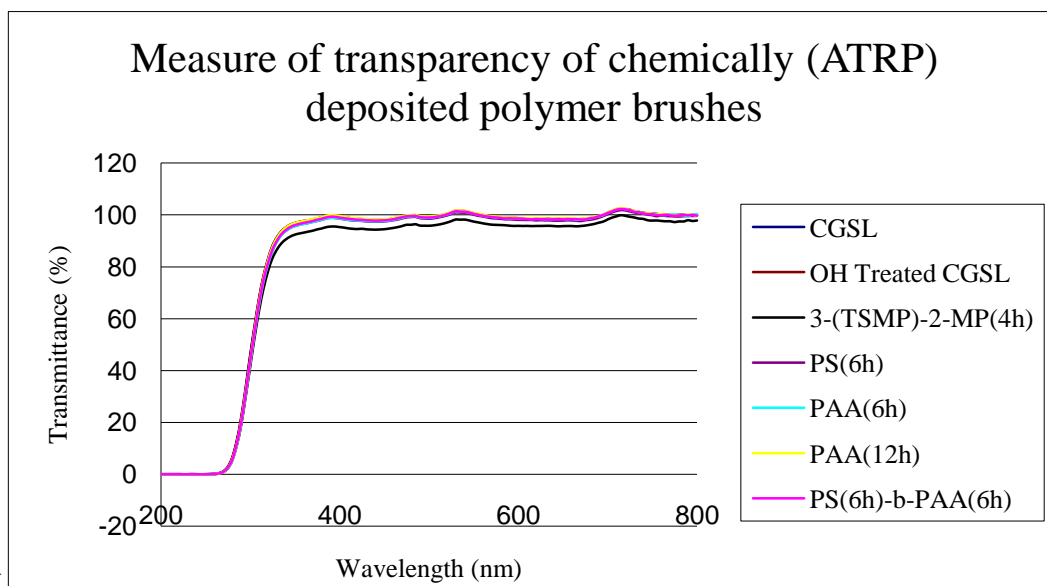
Figure 4.18: Transmittance of ultraviolet-visible light clean glass slide, hydroxylated glass slide, chemically modified glass slides of TMSPBMB ((3-(TSMP)-2-MP) 4 hrs reaction time), PS (6 hours), PAA (6 hours), PAA (12 hours), and PS-*b*-PAA (6 hours).

Although the regional grouping observed in Figure 4.9 was not observed in Figure 4.18, the UV-vis transmittance measurements of PS_{60}-*b*-PAA_{29} brush surfaces fabricated via ATRP also suggest that the surfaces are semi-transparent, which is important for applications in lenses or windows. This observation could mean that grafting density variations were not achieved with ATRP as was the case with LB physical deposition. To confirm this suspicion, fluorescence microscopy imaging was

taken and discussed below.

Fluorescence imaging studies

      Samples listed in Table 4.2 were deposited on hydroxylated, pre-treated glass

slides by ATRP in order to study and compare the surface morphology of both

covalently linked brushes and physisorbed brushes.

Table 4.2: Samples prepared by chemical deposition of anti-biofouling polymers
using ATRP ("grafting from approach")

Sample #	Description
1	Glass - untreated
2	Glass - hydroxylated
3	3-(Trimethoxysilylpropyl)-2-methylproprionate (TMSPBMB)
4	Poly(acrylic acid) brush (6hrs) (PAA)
5	Poly(acrylic acid) brush (12hrs)
6	Polystyrene brush (6hrs)
7	Polystyrene-block-poly(acrylic acid) (PS-*b*-PAA)

Only PS-*b*-PAA fluorescence micrograph is presented here because all the samples

essentially look similar to PS-*b*-PAA micrograph under the fluorescence microscope.

      Therefore, it is difficult to observe any pattern formation or deduce any

grafting density variation information from the fluorescence micrographs of the

chemically deposited brush shown Figure 4.19. Inability to visibly see what is going

on the chemically deposited brushes could also be due to high brush thickness, thus

forming an opaque carpet. In order to study the morphology, we need a more

powerful tool such as atomic force microscope imaging.
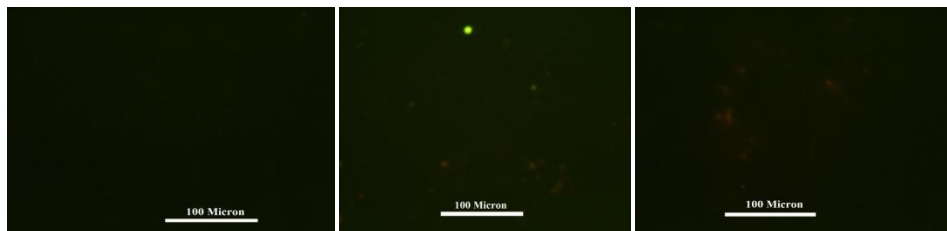
Figure 4.19: Fluorescence micrograph survey of the chemical deposition PS-*b*-PAA - each block was grafted for 6 hours.

Atomic force microscopic (AFM) analysis

Figures 4.20 and 4.21 show the PS-*b*-PAA prepared by Ni, 2010 (MS Thesis) through ATRP (using the same procedure used in this project to prepare the chemically deposited brushes). It is evident that there is no grafting density variation in the film prepared by ATRP. However, we can see nanoscale topography, roughness, and surface micelle formations.
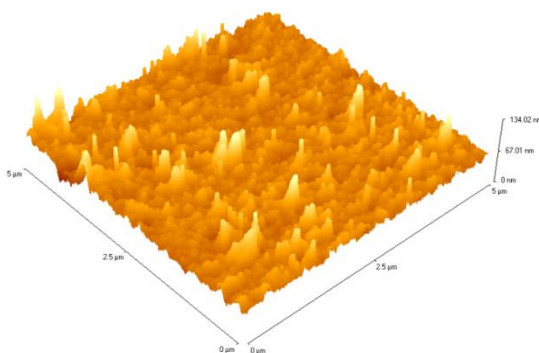
Figure 4.20: AFM Topographic view of PS-*b*-PAA prepared by ATRP using AFM SI$_3$N$_4$ tip (Ni, 2010 (MS Thesis); Jahn Torres, NUWC).
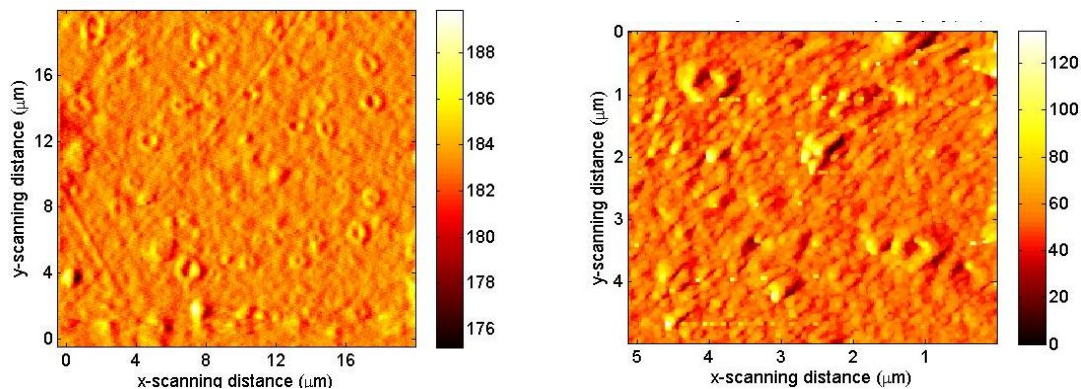
Figure 4.21: AFM Topographic image of PS-*b*-PAA prepared by ATRP using AFM SI$_3$N$_4$ tip (Qian Thesis, 2010; Jahn Torres, NUWC).

Biofouling studies of covalently linked polymer brushes (ATRP)

Bio-adhesion studies were conducted by the Callow laboratory at the University of Birmingham, UK. The results are hereby presented below.

The bar labeled 'Glass' in Figure 4.22 represents the control in the biofouling studies. The densities of attached spores varied with chemical composition of the modified surface and grafting duration. The lower the spore density of a modified surface compare to the glass spore density, the more effective the biofouling coating on that particular modified surface.

Hydroxylated and silane modified glass slides show lower spore settlement density. In the case of the poly(acrylic acid) modified surface, grafting duration of the brush has a direct impact on the film efficiency, that is, the PAA brush grafted for 6 hours shows higher settlement density than the unmodified glass slide while the 12 hours modified glass show almost half the settlement density of the unmodified glass slide.

63
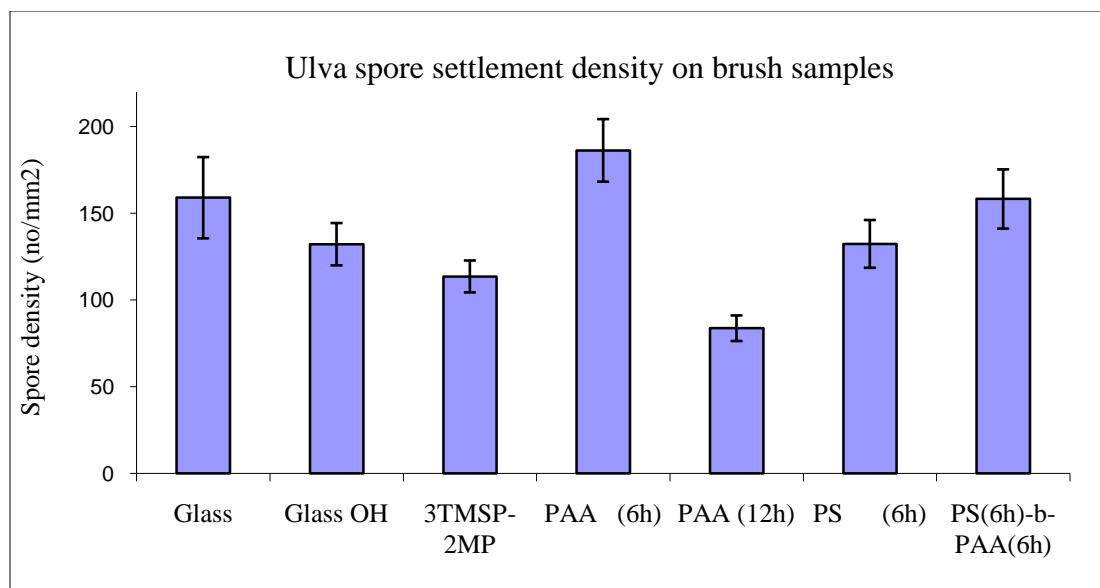
Figure 4.22: The grafting density of attached Ulva spores on polymer brush samples after 45 minutes of settlement. Each point represents the mean from 120 counts on 4 replicate glass slides. Bars show 95% confident limits (Finlay et al, 2011).

Polystyrene surface, a hydrophobic surface, is notorious for allowing settlement of spores (Finlay et al, 2011; Newey et al, 2007; Young et al, 1984). So, the 6 hour PS and 6h-6h of PS-*b*-PAA grafts in Figure 4.22 experienced 83% and 99% spore attachment respectively. This characteristic is supported by the average advancing contact angle measurements in Figure 4.17 where PS has a contact angle of 69.6^o and PS-*b*-PAA has a contact angle of 69.7^o. The attachment of the spores to the PS and PS-*b*-PAA modified surfaces confirmed that poly(tert-butyl acrylate) was not completely hydrolyzed to PAA. It also suggests that the thickness of the brushes needs to be increased by increasing the grafting time. Therefore, an anti-biofouling effective brush may need to be grafted for at least 24 hours.

As at the time of the preparation of this thesis, anti-biofouling studies on the polymer brushes made from physical deposition is underway; hence, the comparison

of the efficiency of the brushes fabricated through ATRP and LB will have to happen at a future date because not biofouling data is available for the LB fabricated brushes at this moment.

CHAPTER 5

CONCLUSIONS

Biofouling adversely affects the environment and has enormous economical impacts. Biocide based antifouling paints were effective in combating fouling but leaching of toxins from the biofouling paints rendered biocide antifouling paints unsuitable. Nanotechnology offers the promise of alternative antifouling coatings that are environmentally benign and efficient against fouling. By engineering surfaces with commercially available polyelectrolyte coatings (PS-*b*-PAA), we were able to fabricate surface that may have anti-biofouling properties through electrostatic and steric repulsive forces.

Furthermore, surface treatment prior to the physical deposition of the polyelectrolyte brush is a critical step that determines the success or failure of anti-biofouling surface fabrication. When polystyrene was allowed to settle as a film on the surface of glass and heated in the vacuum over for 72 hours, then cleaned with chloroform to remove unbounded polystyrene, physically deposition PS_{60}-*b*-PAA_{29} on the surface of glass was successful.

Surface pressure-area isotherm of PS_{60}-*b*-PAA_{29} film revealed that if temperature of the deionized subphase is raised above $20^{o}C$ in the absence of pH adjustment, electrostatic and repulsive force prevent close packing of the polyelectrolyte brushes due to increase in thermal energy. This phenomenon helped us to understand the surface activity of PS_{60}-*b*-PAA_{29} in aqueous environment. In the

presence of salt, charge screening occurred leading to grafting density variation. Increasing the pH of the subphase to a value above the pKa value of PAA should lead to higher grafting density; however, increasing the pH to 7 or 10 with a deposition pressure of 40mN/m instead of 22mN/m suppressed the effect of pH with respect to controlling grafting density. So, at deposition pressure of 40mN/m, the brush at pH 4 should have lower grafting density and indeed exercised slightly lower wettability than the brush at pH 7 and 10.

In order to understand the surface morphology of the polymer brushes, the brushes were viewed under fluorescence microscope: non-hydrate PS_{60}-b-PAA_{29} brush deposited at 22mN/m surface pressure and subphase temperature of up to 25°C (deionized water subphase) organized themselves into long strips or coils of polymer mosaic probably due to collapse of the PAA chains.

However, when the modified slides were hydrated as shown in Figure 4.9, stretching of the PAA block of the copolymer was observed. It can be seen that the thickness of the brush increase due to wetting (evidence of hydrophilic nature of PAA).

The pressure, subphase, and pH were changed in order to study the behaviors of the polymer brush. At basic pH (pH 9.97), the PAA block of the PS_{60}-b-PAA_{29} become ionized (the carboxylic groups of the PAA chain ionized) and acquire negative charges, these result in steric and electrostatic repulsions, as well as, charge screening. It can also be seen in Figure 4.13 that the brush look like dots instead of strand-like appearance that was observed when the film was dry. This dot-like

appearance proved that the PAA blocks have stretched and they are standing upright. Hence, brush density has decreased.

It is impossible to observe any pattern formation or deduce any grafting density variation information from the fluorescence micrographs of the chemically deposited brush shown Figure 4.19. Inability to visibly see what is going on the chemically deposited brushes could also be due to high brush thickness, thus forming an opaque carpet. In order to study the morphology, we need a more powerful tool such as atomic force microscope imaging.

The existence of these three different regions on the UV-vis of the physically deposited brushes, which was not observed in Figure 4.18, the UV-vis transmittance measurements of PS_{60}-b-PAA_{29} brush surfaces fabricated via LB and ATRP method suggest that the surfaces are semi-transparent, which is important for applications in lenses or windows.

Preliminary biofouling studies of surface modified with ATRP deposition shows that grafting duration (hence, thickness) of polyelectrolyte brush has a direct impact on the film efficiency against biofouling, that is, the PAA brush grafted for 6 hours shows higher settlement density than the unmodified glass slide while the 12 hours modified glass show almost half the settlement density of the unmodified glass slide. The attachment of the spores to the PS brushes shows that PS surfaces are not effective anti-biofouling brushes but adhesion of the spores to the PS-b-PAA modified surfaces suggests that the thickness of the brushes needs to be increased by increasing the grafting time. It will also be necessary to increase the hydrolysis time of poly(tert-butyl acrylate) to 8 hours or more. Therefore, for PS-b-PAA brush

surface to be effective against biofouling, it may need to be grafted for at least for 24 hours if ATRP is to be used.

FUTURE WORKS

Physical Deposition: Biofouling studies on physically fabricated polyelectrolyte brushes are underway at URI aquarium where the samples are immersed in sea water pumped directly from the ocean. Future samples will be deposited on full size microscope slides via Langmuir-Schaeffer technique. Quantitative AFM work will also be done to determine brush thickness, grafting density, and adhesive strength of the polymer brush transferred to the substrate's surface.

Chemical Deposition: Sample will be prepared on full size microscope slides with at least 8 hours of hydrolysis of poly(tert-butyl acrylate) to PAA and at least 24 hours of grafting time in order to increase the thickness of the brush to a level sufficient enough to prevent or drastically reduce biofouling and test of such samples will be conducted in Dr. Callow's lab at the University of Birmingham, United Kingdom.

HISTORICAL DEVELOPMENTS IN MONOLAYER SCIENCE
(Roberts, Ed., 1990)

Benjamin Franklin (1706-1790)

Benjamin Franklin, an American elder statesman, applied the principles of observation, investigation, and hypothetical deduction and ushered in the field of monolayer science. His brilliant approach stimulated interest in scientific communities around the world.

While traveling to Europe by sea, Benjamin Franklin observed that oil on water had a peculiar behavior. He used a large pond as his experimental laboratory and spread a teaspoonful of oil (dropwise) on the surface of the water in a pond on a windy day and he observed the formation of a perfect smooth layer of oil on the surface of the water termed monolayer in modern science. Benjamin also realized that some forces of attraction/ repulsion were at play. Finally, he studied the effects of vibration at the oil/water interface.

John Shields (1822-1890)

John Shields was a proprietor of a linen mill in Scotland who performed large scale experiments in Peterhead and Aberdeen Arbors to investigate the wave damping effect of oil on the surface of water. He pumped oil in small quantities to water surface and discovered that the surface of the water was calm despite winds. The effect only lasted for about an hour.

John Aitken (1839-1919)

John Aitken investigated the notorious theory of wave-dampening by oil. In the wake of the massive oil spills such as Exxon Valdez of 1989 and the BP's Deep Water Horizon of 2010 oil spills, it sounds counterintuitive in contemporary time that one should spread oil on the surface of water at sea every time ships travel on the ocean but in the periods between seventeenth and eighteenth century, the commonly held believe was that oil on the surface of the water causes the sea to be calm.

John Aitken devised an instrument that was capable of detecting movement in water that has been subjected to air current after oil has been spread on the surface of such water and found out that oil did not calm water.

Lord Rayleigh (1842-1919)

Lord Rayleigh departed from traditional way of monolayer study that was prevalent at his time by studying the effect of light on monolayer of fatty acid. He shed light on the effect of surfactant or "contaminant" on the surface tension of water as well as the effect of changing area on surface pressure. Furthermore, he had insight that the monolayer formed on water surface had distinct size. He had the idea that it should be possible to measure the thickness of olive oil that he had spread on the surface of water.

Agnes Pockels (1862-1935)

Agnes Pockels was a non-professional science enthusiast who used tin cans in her kitchen to develop the famous Langmuir film balance model. Her trough was

about 70cm x 5cm x 2cm. She made barriers with tin strips. She used the barriers to change the area of the trough by moving the tin strips on the surface of water in her trough. This design also enabled her to clean the trough whenever she needed to do so. Moreover, she could not publish her work because she had no official scientific training. As a result, she wrote letters to Lord Rayleigh describing her methodology which is regarded as central component of monolayer research today.

Furthermore, Lord Rayleigh had to recommend Agnes' work to the British scientific journal, *Nature*, for publication because of her lack of professional training in the field of science. His letter of recommendation was published with Agnes' publication.

Most importantly, Agnes published the first surface pressure-area isotherms and her work paved way for the quantitative work that we do in monolayer science in contemporary times. Her work also helped Lord Rayleigh to appreciate the application of surface tension in monolayer research. Finally, as a result of Agnes' work, Lord was able to calculate the thickness of olive oil monolayer on the water surface and arrived at the same solution with Benjamin Franklin, 1 nm!

Irving Langmuir (1881-1957)

Irvin Langmuir was a Metallurgical Engineer by training whose works led to gas-filled lamps (gas-filled lamps are known for their higher efficiencies and durabilities). He also worked extensively in the area of surface chemistry for which he won the Nobel Prize in Chemistry. Most importantly, Langmuir unified already known but scattered and neglected scientific theories such as the surface nature of

adsorption, the kinetic theory of gases, and the range of intermolecular attractive forces by showing their relative relationships.

Langmuir measured the spreading pressures of thin films, developed the surface film balance, shed light on the molecular orientation at the surface of water on which a monolayer of organic substance has been spread, confirmed the existence of short-range forces, and finally, he explained why some molecules did not form monolayer films.

Katharine Blodgett (1898-1979)

Katharine Blodgett was first in many things such as first woman to work on the research staff at General Electric, the first person to obtain a doctorate degree from the Cavendish Laboratory in Cambridge, England in UK. She was also the first person to transfer fatty acid monolayer film on to a solid substrate such as glass slides. In her honor, any monolayer(s) transferred to solid substrate is/are known as Langmuir-Blodgett film(s). Finally, Katharine's attention was later directed to studying the optical properties of multilayer films.

APPENDIX B

MONOLAYER CHARACTERIZATION

Surface Pressure-Area Isotherm (Roberts, 1990; Petty, 1996)

Molecules within a liquid have certain extent of attractions for each other. This extent of attraction is referred to as cohesion. By comparison, molecules within a liquid have equal attraction from all directions compared to molecules at the surface of the liquid, which experience disproportionate attractions because of interaction with air on one side and interaction with molecules within the liquid on the other side.

Essentially, the molecules at the surface of a liquid experience much greater attractive forces towards the liquid than toward the air molecule. As a result, there is effective, prevailing attraction towards the liquid aggregate such that the air-water boundary automatically lowers its area and shrinks as a result.

The activities, as well as, the forces that are in play on the surface of the liquid and within the bulk of the liquid lead to a situation where the liquid often has excess free energy. The excess free energy is called surface tension which can be expressed thermodynamically according to the following mathematical expression:

$$\gamma = \left(\frac{\Delta G}{\Delta S}\right)_{T,P,n_i}$$

Where G represents the free energy, S is the surface area. The temperature, pressure, and composition (n_i) are held constant.

Furthermore, hydrogen bonding – notorious for its strength - forms loose networks especially in aqueous environment. The networks formed often undergo

manipulation on the surface of the liquid bulk by actions such as compression of barriers of the Langmuir-Blodgett trough to reduce area and addition of surfactant to the surface of the subphase. Other intermolecular forces also exit in the aqueous subphase because of the polar nature of water. The overall effect of these intermolecular interactions is high surface tension.

The strength of the surface tension is reduced when temperature is increased and surfactants or contaminants are spread on the surface of the subphase. Hence surface pressure is observed because of the difference in environment between the molecules on the surface and those within the bulk of the subphase. It is therefore possible to quantify the surface pressure according to the following mathematical expression:

$$\pi = \gamma_o - \gamma$$

where π is the surface pressure, γ_o is the surface tension of pure deionized water, and γ is the surface tension of water after the spreading of the surfactant. It should be noted that the maximum obtainable surface pressure on water surface is 73mN/m at 20^oC, however, it is could be lower in practice.

In monolayer science, surface pressure-area isotherm was the fundamental tool used in understanding the surface activities of surfactants at air/water interface. Agnes Pockels was the first person to use π-area isotherm in 1893 in analyzing oil on water surface (Roberts, 1990).

Surface pressure-area isotherm is a 2-dimentional graph (Figure B1) that shows the relationship between surface pressure on the vertical axis and the

area/molecule (A^2) on the horizontal axis. It can be divided into the sections called 'phases' named synonymously according to the three phases of matter's existence.
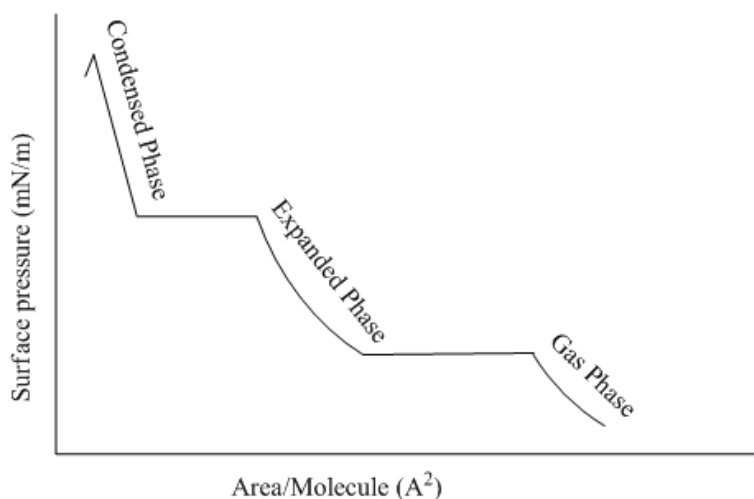
Figure B1: Typical surface pressure-area isotherm of Langmuir Monolayer.

In the gas phase, the molecules of the surfactant have enough space between them such that intermolecular interactions takes place without one molecule interfering with the other, thus they exert very small or negligible force on one another. In addition, the molecules align themselves in a random manner on the surface of the subphase. However, as the area occupied by the monolayer is reduced (barrier compression), the hydrophobic tails start to interact with each other. As the hydrophobic tails are brought even closer, then the interaction will become significant resulting in rise in surface pressure until a constant pressure is observed. This constant pressure ushers in the extended phase and it signifies co-existence of two phases, that is, gas phase and expanded phase. This is a first order thermodynamic transition.

In reality, not all surfactants have all the three phases. Figure B2 is the pressure-area isotherm of PS_{60}-b-PAA_{29} in which the three phases are not observed whereas Figure B3 shows the surface-pressure area isotherm of DPPC with all the three phase.
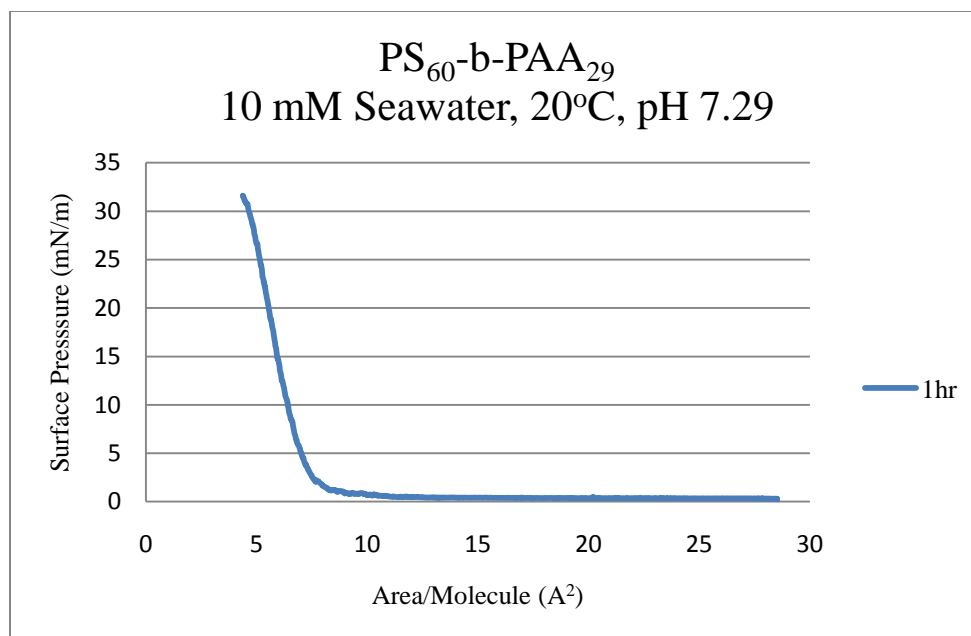
Figure B2: Surface pressure-area Isotherm of PS_{60}-b-PAA_{29} at $20^{o}C$ after 1 hr of spreading on the surface of the monolayer.

The next phase observed is the expanded phase. This phase corresponds to the liquid phase. In order to explain the expanded phase, it will be necessary to refer to the surface pressure-area isotherm of specific surfactants such as PS_{60}-b-PAA_{29} and Dipalmitoylphosphatidylcholine.

In Figure B2, the plateau occurs at about 1mN/m afterwards, the expanded phase appears. The case is the same in Figure B3; the constant pressure region
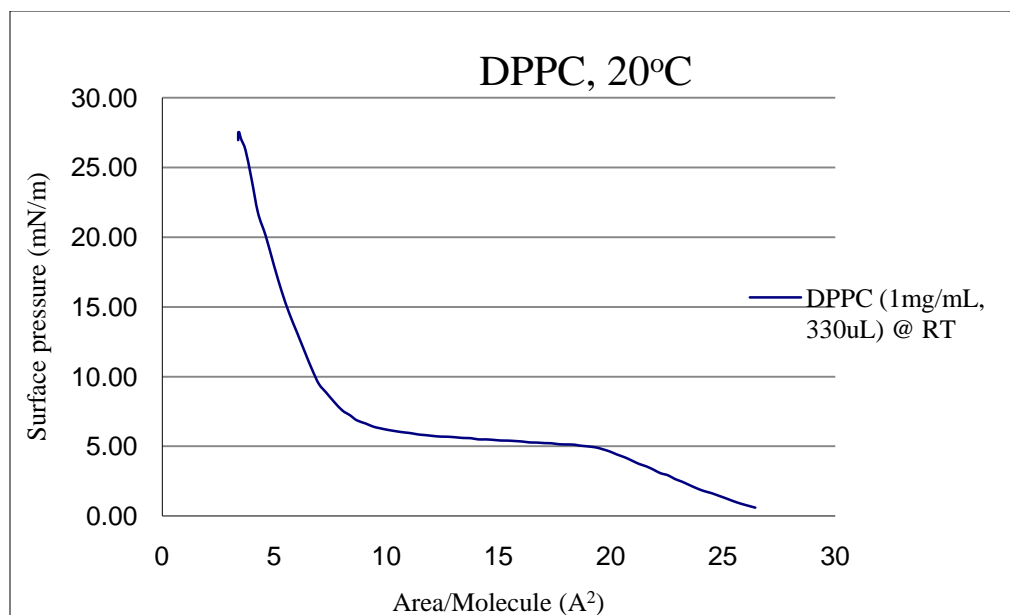
Figure B3: Surface pressure-area isotherm of dipalmitoylphosphatidylcholine (DPPC) at room temperature.

(steadily increasing), then the plateau and finally the expanded phase. These slight differences between the ideal surface pressure-area isotherm and the isotherms for actual surface active agent, as well as, the differences between the isotherms among various surfactants may be due to difference in the length of chain composition of the hydrophobic tails, higher order thermodynamic transition, and effect of residual solvent molecules at the interface of the subphase.

After the expanded phase, another first or higher order thermodynamic transition signified by a constant pressure region or lack thereof ushers in the condensed phase. However, as with the gas and expanded phases, the condensed phase is not always observed in all the monolayer materials.

The factors that contribute to the variations in the expanded to condensed phase transition include the length of the hydrocarbon chain in the hydrophobic tail

and temperature. Generally speaking, decreasing the chain length of hydrocarbon tail leads to an increase in the surface pressure of the phase transition. Also increase in temperature has the same effect (Petty, 1996). At the molecular level, a decrease in chain length leads to diminished intermolecular Van der Waals' forces. Moreover, if the temperature is reduced, the result is a decrease in thermal motion of the molecules within the film. The combined effect of the changes mentioned above result in the formation of the condensed phase.

Sometimes, there may be direct transition between the gas phase and the condensed phase because of extremely long hydrocarbon tail length.

Atomic force microscopy

Atomic force microscopy was developed in 1986 by Binnig, Quate, and Gerber. It is a microscopic method that allows researchers to see and quantify surface structures with extraordinary resolution and accuracy. Surfaces whose structures can be investigated by AFM range from solid materials to microorganisms to macromolecules. One great advantage of using AFM for surface characterization is that it is non-destructive and that is why it is suitable in measuring soft surfaces and biological molecules. It can measure samples between 5 nm to 250 μm (or more) in size. The figure below shows the linear scale of different microscopes used in material science.
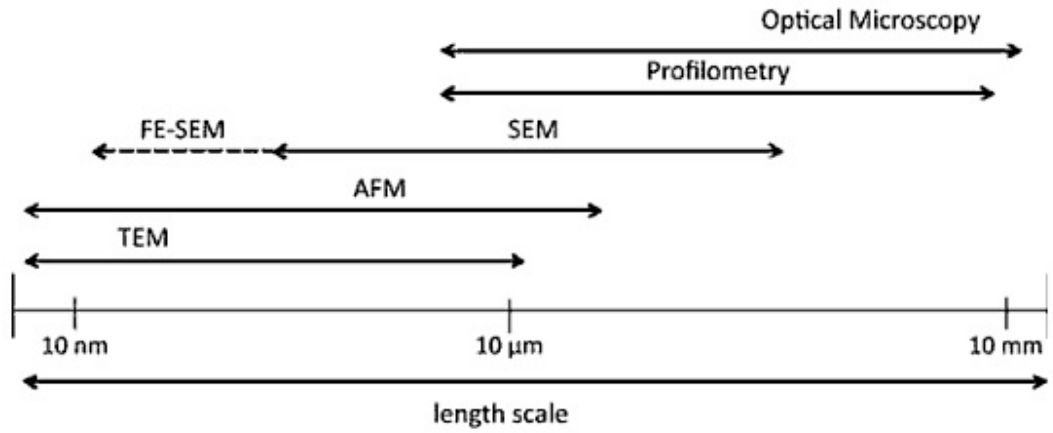
Figure B4: Scale of measure of various microscopes in material science (Eaton et al, 2010)

Figure B5: Atomic force microscope.

AFM takes surface measurement by scanning the tip of the cantilever on a surface resulting in an attractive or a repulsive interplay with the surface. As a result of these interactions, the tip attached to a cantilever experiences a force which causes the cantilever to bend. A laser beam off the cantilever detects the deflection of the

cantilever causing the degree of the laser beam to be translated to image in terms of height or topography (Kolasinski, 2008).

Ultraviolet-Visible Spectroscopy

This is a technique in which the ability of electron to be excited and move between energy levels is utilized. These energy levels have direct correlation to the molecular orbital of the systems. Specifically, UV-vis spectroscopy takes advantage of electronic transitions involving π orbitals and lone pair electrons to identify conjugated systems which have stronger absorptions. The wavelength of ultraviolet light is 200-400nm while that of visible light is 400-800nm.
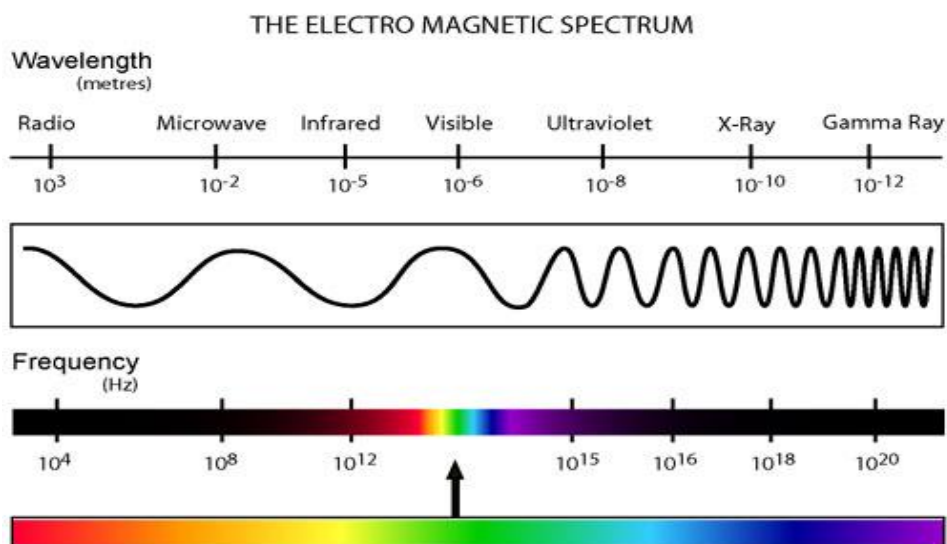
Figure B6: The electromagnetic spectrum adapted from http://sciencejunkies.com/page/3/. Ultraviolet-Visible Spectroscopy operates within the ultraviolet-visible light region of the electromagnetic spectrum.

Thus for a substance to be qualified for testing using UV-vis technique, it must have uninterrupted conjugated double, triple or a mixture of both bonds along a stretch of the molecule. Therefore, the smallest number of molecule of a material that can absorb electromagnetic radiation is called the chromophore.

In principle, the lowest transition of energy occurs between highest occupied molecular orbital (HOMO) and the lowest unoccupied molecular orbital (LUMO) in the ground state. For electrons to move from HOMO to LUMO, electromagnetic radiation must be absorbed, this event causes electrons to be excited to the LUMO. It should be noted that the more unsaturated the substance under test is the smaller the HOMO-LUMO spacing and the change in energy required and consequently, the lower the frequency which means the longer the wavelength.
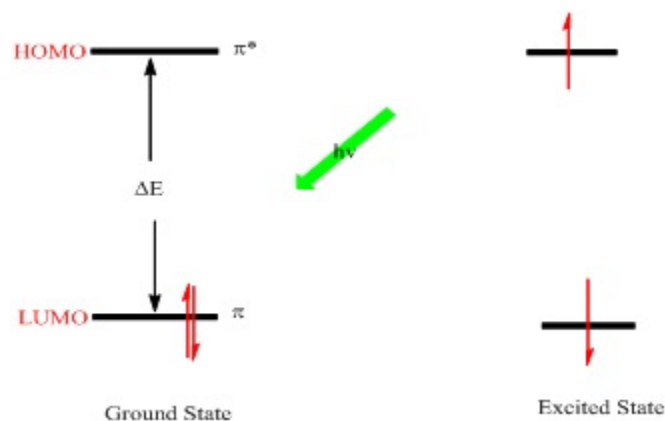
Figure B7: The molecular orbital energy representation of ground state and excited state of two electrons in a molecule.

The general outline of a UV-visible spectrometer can be seen below. An attempt is hereby made to briefly describe the optical principle of UV-vis spectrophotometer. Light from sources are filtered are they enter the monochromator.

Hence, as the light exits the monochromator, it becomes monochromatic light. The monochromatic light then illuminates the sample. A detector then measures the amount of light that passes through the sample.
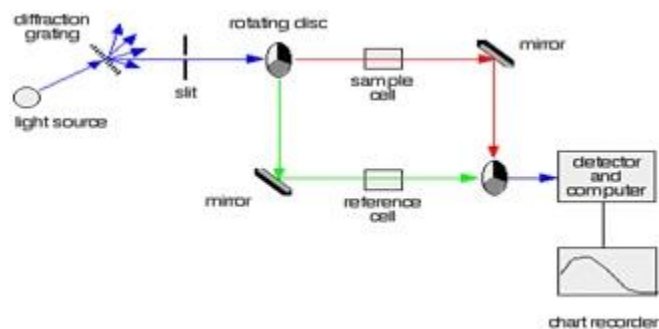
Figure B8: The general outline of UV-visible light spectrometer adapted from http://www.chemguide.co.uk/analysis/uvvisible/spectrometer.html#top.

APPENDIX C

VOLUME CALCULATION FOR PS$_{60}$-b-PAA$_{29}$ MONOLAYER

Part 1

$Total\ Volume\ of\ polymer\ needed = \#\ of\ monomer * V_{polymer}$

$PAA\ VdW\ Volume = 9.81 * 10^{-23}\ cm^3/molecule$

$V = 4/3\ \pi R^3$

$R = ((3 * 29 * 9.8 * 10^{-23})/4\pi)^{1/3}$

$\quad = 8.79 * 10^{-8} cm * 10^7\ nm/cm * molecule$

$\quad = 0.879\ nm/molecule$

$Area = \pi R^2 = \pi * 0.879^2 = 2.43\ nm^2/molecule$

$Assume\ Trough\ Area = 100 cm^2$

$\#of\ PAA\ molecules\ to\ coat\ surface = \dfrac{100\ cm^2}{(2.43\ nm^2/molecule)(1 * 10^{-7cm}/nm)^2}$

$$= 4.12 * 10^{15} molecules(needed)$$

$Stock\ Solution\ content = 1 mg/mL$

$mmole\ of\ PAA\ in\ stock\ soln = (1mg/mL)(mmole/2106mg) = 0.47mmol/L$

$= (4.7 * 10^{-4} mmole/mL)(6.022 * 10^{23} molecules/mole)(mole/1000mmole)$

$= 2.86 * 10^{17}\ molecules/mL$

$Vol\ of\ PAA\ needed = 4.12 * 10^{15} molecules/2.86 * 10^{17}\ molecules/mL$

$$= 0.014mL\ or\ 14\mu L$$

Part 2

$Styrene\ VdW\ Volume = (6.6250 * 10^{-2}\ m^3/kmole)(kmole/1000mole)$

$= (60 * 6.6250 * 10^{-5}\ m^3/mole)(10^6\ cm^3/m^3)(mole/6.022 * 10^{23}molecules)$

$Styrene\ VdW\ Volume = 6.600797 * 10^{-21}\ cm^3/molecule$

$V = 4/3\ \pi R^3$

$R = ((3 * 6.600797 * 10^{-21})/4\pi)^{1/3}$

$= 1.164 * 10^{-7}cm * 10^7\ nm/cm * molecule$

$= 1.164\ nm/molecule$

$Assume\ Trough\ Area = 100cm^2$

$\#of\ PS\ molecules\ to\ coat\ surface = \dfrac{100\ cm^2}{(1.164\ nm^2/molecule)(1 * 10^{-7cm}/nm)^2}$

$= 8.59 * 10^{15}molecules(needed)$

$Stock\ Solution\ content = 1mg/mL$

$mmole\ of\ PAA\ in\ stock\ soln = (1mg/mL)(mmole/6213mg)$

$= 1.6095 * 10^{-4}mmol/L$

$= (1.6095 * 10^{-4}mmole/mL)(6.022$

$* 10^{23}molecules/mole)(mole/1000mmole)$

$= 9.693 * 10^{16}\ molecules/mL$

$Vol\ of\ PS\ needed = 8.591 * 10^{15}molecules/9.693 * 10^{16}\ molecules/mL$

$= 0.08864mL\ or\ 88.64\mu L$

Area/molecule calculation of PS_{60}-*b*-PAA_{29} monolayer at fully opened and fully closed barrier positions

Table C1: Area/molecule calculation of PS_{60}-*b*-PAA_{29} at air/water and air/sea water interface.

Temp (°C)	Area @full open cm²	1/a_o @full open molec/A²	1/a_o @full open molec/A²	a_0 (A²/molec)	a_0 (nm²/molec)
0	72.10	9.04E+13	9.04E-03	110.66827	1.10668
15	72.09	9.04E+13	9.04E-03	110.65292	1.10653
20	72.17	9.03E+13	9.03E-03	110.77572	1.10776
25	72.11	9.03E+13	9.03E-03	110.68362	1.10684
Temp (°C)	Area @ collapse cm²	1/a_o @ collapse molec/A²	1/a_o @ collapse molec/A²	a_0 (A²/molec)	a_0 (nm²/molec)
0	18.12	3.60E+14	3.60E-02	27.81289	0.27813
15	18.13	3.59E+14	3.59E-02	27.82824	0.27828
20	18.11	3.60E+14	3.60E-02	27.79754	0.27798
25	18.12	3.60E+14	3.60E-02	27.81289	0.27813
pH	Area @full open cm²	1/a_o @full open molec/A²	1/a_o @full open molec/A²	a_0 (A²/molec)	a_0 (nm²/molec)
4.01	72.20	9.0235E+13	9.02E-03	110.82176	1.10822
7.06	72.11	9.03476E+13	9.03E-03	110.68362	1.10684
9.96	71.96	9.05359E+13	9.05E-03	110.45338	1.10453
pH	Area @ collapse cm²	1/a_o @ collapse molec/A²	1/a_o @ collapse molec/A²	a_0 (A²/molec)	a_0 (nm²/molec)
4.01	18.16	3.58754E+14	3.59E-02	27.87	0.27874
7.06	18.13	3.59347E+14	3.59E-02	27.83	0.27828
9.96	18.11	3.59744E+14	3.60E-02	27.80	0.27798

BIBLIOGRAPHY

Almeida, E., Diamantino, T. C., and Sousa, O. D. (2007). "Marine paints: The particular
case of antifouling paints." Progress in Organic Coatings **59**: 2-20.

Amiji, M., Park, K. J. (1993). "Surface modification of polymeric biomaterials with
Poly(ethylene 16 oxide), albumin, and heparin for reduced thrombogenicity."
J Biomater Sci Polym Edn (4): 217-234.

Anderson, C. D. (1995). "Tin vs Tin free Antifoulings." Cda.swsconf: 1-12.

Anderson, C. D. (1998). IBC UK. United Kingdom, IBC UK Conferences Limited**:**
1-12.

Awad, M. M. "Fouling of heat transfer surfaces ": 505-541.

Baghdachi, J. (2009). Smart coatings. ACS Symposium Series Washington, DC,
American Chemical Society.

Ballauff, M., Borisov, O. (2006). "Polyelectrolyte brushes." Current Opinion in
Colloid & Interface Science **11**: 316-323.

Bertram, V. (2000). Past, present and future prospects of antifouling. Proceedings of
the 32nd WEGEMT School on Marine Coatings, Plymouth, UK.

Brooksa, S., Thomasa, K. V. (2010). "The environmental fate and effects of
antifouling paint biocides." Biofouling **26**(1): 73-88.

Callow, J. An Integrated Project to study and develop new nano-structured surfaces
for the control of biofouling in aquatic environments. Birmingham, University
of Birmingham 2.

Callow, J. (2007). Advanced nanostructured surfaces for the control of biofouling.
Birmingham, University of Birmingham.

Carman, M. L., Estes, T. G., Feinberg, A. W., Schumacher, J. F., Wilkerson, W.,
Wilson, L. H., Callow, M. E., Callow, J. A., and Brennan, A. B. (2006).
"Engineered antifouling microtopographies – correlating wettability with cell
attachment." Biofouling: 1-11.

CEPE-AWG (1999). Utilisation of more 'environmentally friendly' antifouling
products. EC project No 96/559/3040/DEB/E2. Phase 1 - final report. C. A.
W. Group. Brussels.

Chambers, L. D., Stokes, K. R., Walsh, F. C., and Wood, R. J. K. (2006). "Modern approaches to marine antifouling coatings." Surface and Coatings Technology **201**: 3642-3652.

Chamsaz, M., Khasawneh, I. M., and Winefordner, J. D. (1988). "Speciation and determination of tin(IV) and organotin compounds in sea-water by hydride generation—atomic-absorption spectrometry with an electrically heated long absorption cell " Talanta **35**(7): 519-523.

Chang, Y., Chen, S., Zhang, Z., and Jiang, S. (2006). "Highly protein-resistant coatings from well-defined diblock copolymers containing sulfobetaines." Langmuir **22**(5): 2222-2226.

Chapman, R. (2003). Personal Communication.

Chapman, R. G., Ostuni, E., Takayama, S., Holmlin, R. E., Yan, L., and Whitesides, G. M. (2000). "Surveying for surfaces that resist the adsorption of proteins." J. Am. Chem. Soc. **122**: 8303-8304.

Chibowski, S., Paszkiewicz, M. (2006). "Polyacrylic acid (PAA) adsorption on alumina (Al2O3) surface: Influence of sodium dodecyl sulfide (SDS) on adsorption in PAAA-SDS-Al2O3 system." Physicochemical Problems of Mineral Processing **40**: 175-184.

Currie, E. P. K., Sieval, A. B., Fleer J. G., and Stuart, M. A. (2000). "Polyacrylic acid brushes: Surface pressure and salt-induced swelling." Langmuir **16**: 8324-8333.

De Gennes, P. G., Raphael, E. (1992). "Rubber-rubber adhesion with connector molecules." J Phys Chem **96**: 4002–4007.

De Gennes, P. G., Ji, H. (1993). "Adhesion via connector molecules: the many-stitch problem." Macromolecules **26**: 520-525.

Drechsler, A., Grundke, K. (2005). "The influence of electrolyte ions on the interaction forces between polystyrene surfaces." Colloids and Surfaces A: Physicochem. Eng. Aspects **264**: 157-165.

Eaton, P., West, P. (2010). Atomic force microscopy. New York, Oxford University Press.

Etienne, O., Picart, C., Taddei, C., Haikel, Y., Dimarcq, J. L., Schaaf, P., Voegel, J.-C., Ogier, J. A., and Egles, C. (2004). "Multilayer polyelectrolyte films functionalized by insertion of defensin: a new approach to protection of implants from bacterial colonization." Antimicrobial Agents and Chemotherapy **48**: 3362.

Evans, D. F., Wennerstrom, H (1999). <u>The colloidal domain</u>. New York, Wiley-VCH.

Fan, X., Lin, L., and Messersmith, P. B. (2006). "Cell fouling resistance of polymer brushes grafted from Ti substrates by surface-initiated polymerization: effect of ethylene glycol side chain length." <u>Biomacromolecules</u> **7**: 2443-2448.

Francolini, I., Norris, P., Piozzi, A., Donelli, G., and Stoodley, P. (2004). "Usnic acid, a natural antimicrobial agent able to inhibit bacterial biofilm formation on polymer surfaces." <u>Antimicrobial Agents and Chemotherapy</u> **48**(11): 4360-4365.

Gabriel, M., Nazmi, K., Veerman, E. C., Niew Amerongen, A. V., Zentner, A., Gabriel, M., Nazmi, K., and Veerman, E. C. (2006). "Preparation of, 548-550. LL-37-grafted titanium surfaces with bactericidal activity." <u>Bioconjugate Chem</u> **17**:

Gebhardt, J. E., Fuerstenau, D. W. (1983). "Adsorption of polyacrylic acid at oxide/water interfaces." <u>Colloids and surfaces</u> **7**: 221-231.

Genzer, J., Efimenko, K. (2006). "Recent developments in superhydrophobic surfaces and their relevance to marine fouling: a review." <u>Biofouling</u> **22**(5): 339-360.

Gitlitz, M. H., M&T chemicals, Incorporated (1981). "Recent developments in marine antifouling coatings." <u>J. Coating Technology</u> **53**(678): 46-52.

Glinel, K., Jonas, A. M., Jouenne, T., Leprince, J., Galas, L., and Huck, W. T. (2009). "Antibacterial and antifouling polymer brushes incorporating antimicrobial peptide." <u>Bioconjugate Chem</u> **20**: 71-77.

Guyomard, A., De, E., Jouenne, T., Malandain, J.-J., Muller, G., and Glinel, K. (2008). "Incorporation of a hydrophobic antibacterial peptide into amphiphilic polyelectrolyte multilayers: A bioinspired approach to prepare biocidal thin coatings." <u>Ad . Funct. Mater</u> **18**: 758.

Howell, D. J., Evans, S. M. (2009). "Antifouling materials." <u>Encyclopedia of Ocean Sciences</u>: 203-2010.

Huang, Y., Iwata, M., Usami, M., and Ueda, K (1999). <u>A Study on the antifouling technique through seawater electrolysis on structural surface</u>. Proceedings of the Ninth International Offshore and Polar Engineering Conference, Brest, France.

Hur, J., Witte, K. N., Sun, W., and Won, Y.-Y. (2010). "On the Origins of the Salt-Concentration-Dependent Instability and Lateral Nanoscale Heterogeneities of Weak Polyelectrolyte Brushes: Gradient Brush Experiment and Flory-Type Theoretical Analysis." <u>Langmuir</u> **26**(3): 2021-2034.

Hussain, S. A. Langmuir-Blodgett Films a unique tool for molecular electronics**: 1-9.

Institution, W. H. O. Marine fouling and its prevention, U. S. Naval Institute (PWH)

Iselin, C. O. D. (1952). Marine fouling and its prevention. Annapolis, Woods Hole Oceanographic Institution (WHOI).

Jain, P., Dai, J., Grajales, S., Saha, S., Baker, G. L., and Bruening, M. L. (2007). "Completely aqueous procedure for the growth of polymer brushes on polymeric substrates." <u>Langmuir</u> **23**: 11360-11365.

Joanny, J. F. (1992). "Lubrication by molten polymer brushes." <u>Langmuir</u>(8): 989–995.

Jones, D. S., Brendan. C. O., Muldoon, A., Woolfson, A. D., Andrews, G. P., and Sanderson, F. D. (2008). "Physicochemical characterization of bioactive polyacrylic acid organogels as potential antimicrobial implants for the buccal cavity." <u>Biomacromolecules</u> **9**: 624-633.

Jones, D. S., Muldoon, B. C. O., Woolfson, A. D., Andrews, G. P., and Sanderson, F. D. (2008). "Physicochemical characterization of bioactive polyacrylic acid organogels as potential antimicrobial implants for the buccal cavity." <u>Biomacromolecules</u> **9**: 624-633.

Kolasinski, K. W. (2008). <u>Surface science: foundations of catalysis and nanoscience</u>, John Wiley and Sons.

Kondur, V. (2010). Static and dynamic contact angle measurement on rough surfaces using sessile drop profile analysis with application to water management in low temperature fuel cells. <u>Department of Mechanical Engineering</u>. Michigan, Michigan Technological University. **Master of Science:** 86.

Krishnan, S., Wang, N., Ober, C. K., Finlay, J. A., Callow, M. E., Callow, J., A., Hexemer, A., Sohn, K. E., Kramer, E. J., and Fischer, D. A. (2006). "Comparison of the fouling release properties of hydrophobic fluorinated and hydrophilic PEGylated block copolymer surfaces: attachment strength of the diatom Navicula and the green alga Ulva." <u>Biomacromolecules</u> **7**(5): 1449-1462.

Lichtman, J. W., Conchello, J. (2005). "Fluorescence microscopy." <u>Nature methods</u> **2**(12): 910-919.

Lu, Y., Wittemann, A, Ballauff, M (2009). "Supramolecular structures generated by spherical polyelectrolyte brushes and their application in catalysis." <u>Macromolecular Rapid Communications</u> **30**(9-10): 806–815.

Magin, C. M., Cooper, S. P., and Brennan, A. B. (2010). "Non-toxic antifouling strategies." <u>Materials Today</u> **13**(4).

Muller, P., Sudre, G., Theodoly, O (2008). "Wetting transition on hydrophobic surfaces covered by polyelectrolyte brushes." <u>Langmuir</u> **24**: 9541-9550.

Newey, L. J., Caten, C. E., and Green, J. R. (2007). "Rapid adhesion of stagonospora nodorum spores to a hydrophobic surface requires pre-formed cell surface glycoproteins." <u>Mycological Research</u> **111**(11): 1255-1267

Ni, Q. (2010). Polyelectrolyte polymer brushes as antifouling coatings. <u>Chemical Engineering</u>. Kingston, The University of Rhode Island. **Master of Science:** 109.

Okochi, M., Nakamura, N., and Matsunaga, T. (1995). "Electrochemical disinfection Of marine bacteria using an electro-conductive paint and its application for prevention of biofouling." <u>Denki Kagaku</u> **63**: 1200-1204.

Ostuni, E., Chapman, R. G., Holmlin, R. E., Takayama, S., and Whitesides, G. M. (2001). "A Survey of structure property relationships of surfaces that resist the adsorption of protein." <u>Langmuir</u> **17**: 5605-5620.

Perrino, C., Lee, S., Choi, S. W., Maruyama, A, and Spencer, N. D. (2008). "A biomimetic alternative to poly(ethylene glycol) as an antifouling coating: resistance to nonspecific protein adsorption of poly(l-lysine)-graft-dextran." <u>Langmuir</u> **24**(16): 8850–8856.

Petty, M. C. (1996). <u>Langmuir-Blodgett films: an introduction</u>, Cambridge University Press.

Ranke, J., Jastorff, B. (1999). "Multidimensional risk analysis of antifouling biocides." <u>Environmental Science and Pollution Res.</u> **7**(2): 2000.

Roberts, G., Ed. (1990). <u>Langmuir-Blodgett films</u>. New York, Plenum Press.

Rowe-Konopacki, M. D., Boyes, S. G. (2007). "Synthesis of surface initiated diblock copolymer brushes from flat silicon substrates utilizing the RAFT polymerization technique." <u>Macromolecules</u> **40**: 879-888.

Samuel, U., Guggenbichler, J. P. (2004). "Prevention of catheter-related infections: the potential of a new nano-silver impregnated catheter." <u>Int. J. Antimicrob</u> **23**: 75-78.

Schultz, M. P., Bendick, J. A., Holm, E. R.,and Hertel, W. M. (2010). "Economic Impact of biofouling on a naval surfave ship." <u>Biofouling: The Journal of Bioadhesion and Biofilm Research</u> **27**(1): 1029-2454.

Senaratne, W., Andruzzi, L., and Ober, C. K. (2005). "Self-assembled monolayers and polymer brushes in biotechnology: current applications and future perspectives." <u>Biomacromolecules</u> **6**: 2427–2448.

Sohn, E., Kim, B. G., Chung, J., and Lee, J. (2011). "Wettability of the Morphologically and compositionally varied surfaces prepared from blends of well ordered comb-like polymer and polystyrene." <u>Journal of Colloid and Interface Science</u> **354**: 650-661.

Stupak, M. E., Garcia, T. M., and Perez, M. C. (2003). "Non-toxic alternative Compounds for marine antifouling paints." <u>International biodeterioration & biodegradation</u> **52**(1): 49-52.

Swain, G. (1998). <u>Redefining antifouling coatings</u>. Proceeding of the international symposium on sea water drag reduction, The Naval Undersea Warfare Center, Newport, RI.

Tanner, S. (2005). "Call for papers." <u>Progress in Organic Coatings</u> **54**: 139-140.

Tay, S. N., Yang, C. (2006) Assessment of the hydro-ball condenser tube cleaning system. **Volume**, DOI:

Tompkins, H. G. (1992). <u>A User's Guide to Ellipsometry</u> Academic Press.

Treat, N. D., Ayres, N., Boyes, S. G., and Brittain, W. J. (2006). "A facile route to poly(acrylic acid) brushes using atom transfer radical polymerization." <u>Macromolecules</u> **39**(1): 26-29.

Wang, J., Somasundaran, P. (2006). "Reversible conformational behavior of poly(acrylic acid) LB film with changes in pH, ionic strength and time " <u>Colloids and Surfaces A: Physicochemical and Engineering Aspects</u> **273**(1-3): 63-69.

Wang, S., Zhu, Y. (2003). "Facile method to prepare smooth and homogeneous polymer brush surfaces of varied brush thickness and grafting density." <u>Langmuir</u> **25**(23): 13448-13455.

Wu, T., Gong, P., Szleifer, I., Vlcek, P., Subr, V., and Genzer, J. (2007). "Behavior of surface-anchored poly(acrylic acid) brushes with grafting density gradients on solid substrates: 1. Experiment." <u>Macromolecules</u> **40**: 8756-8764.

Xu, C., Wayland, B. B., Fryd, M., Winey, K. I., and Composto, R. J. (2006). "pH-responsive nanostructures assembled from amphiphilic block copolymers." <u>Macromolecules</u> **39**(18): 6063-6070.

Yebra, D. M., Kiil, S., and Dam-Johansen, K. (2004). "Antifouling technology—past, present and future steps towards efficient and environmentally friendly antifouling coatings." Progress in Organic Coatings **50**: 75-104.

Young, D. H., Kauss, H. (1984). "Adhesion of Colletotrichum lindemuthianum spores to phaseolus vulgaris hypocotyls and to polystyrene." Applied and Environmental Microbiology. **47**(4): 616-619.

Zhang, Z., Finlay, J. A., Wang, L., Gao, Y., Callow, J. A., Callow, M. E., and Jiang, S. (2009). "Polysulfobetaine-grafted surfaces as environmentally benign ultralow fouling marine coatings." Langmuir **25**(23): 13516-13521.

Zhu, Y., Shi, M., Wu, X., and Yang, S. (2007). "Amphiphilic copolymer grafted "smart surface" enhanced by surface roughness." Journal of Colloid and Interface Science **315**: 580-587.